Solid Earth
Discussions
Open Access
EGU

1 # Interactions of plutons and detachments,

2 # comparison of Aegean and Tyrrhenian granitoids

3

4

5 **Laurent Jolivet** [1], **Laurent Arbaret** [2,3,4], **Laetitia Le Pourhiet** [1], **Florent Cheval-**

6 **Garabedian** [2,3,4], **Vincent Roche** [1], **Aurélien Rabillard** [2,3,4], **Loïc Labrousse** [1]

7

8 [1] Sorbonne Université, CNRS-INSU, Institut des Sciences de la Terre Paris, ISTeP UMR 7193, F-75005

9 Paris, France

10 [2] Université d'Orléans, ISTO, UMR 7327, 45071, Orléans, France

11 [3] CNRS/INSU, ISTO, UMR 7327, 45071 Orléans, France

12 [4] BRGM, ISTO, UMR 7327, BP 36009, 45060 Orléans, France

13

14 **Abstract:** Back-arc extension superimposed on mountain belts leads to distributed normal

15 faults and shear zones, interacting with magma emplacement in the crust. The composition of

16 granitic magmas emplaced at this stage often involves a component of crustal melting. The

17 Miocene Aegean granitoids were emplaced in metamorphic core complexes (MCC) below

18 crustal-scale low-angle extensional shear zones and normal faults. Intrusion in such contexts

19 interacts with extension and shear along detachments, from the hot magmatic flow within the

20 pluton root zone to the colder ductile and brittle deformation along the detachment. A

21 comparison of the Aegean plutons with the Elba Island MCC in the back-arc region of the

22 Apennines subduction shows that these processes are characteristic of pluton-detachment

23 interactions in general and we discuss a conceptual emplacement scenario, tested by numerical

24 models. Mafic injections within the partially molten lower crust above the hot asthenosphere

25 trigger the ascent within the core of the MCC of felsic magmas, controlled by the strain

26 localization on persistent crustal scale shear zones at the top that guide the ascent until the brittle

27 ductile transition is reached during exhumation. Once the system definitely enters the brittle

28 regime, the detachment and the upper crust are intruded while new detachments migrate upward

29 and in the direction of shearing. Numerical models reproduce the geometry and the kinematic

30 evolution deduced from field observations.

31

32

33

1. Introduction

In the deep parts of orogens, the flow of melts is coupled with ductile deformation and controlled by buoyancy and tectonic forces (Brown, 1994; Brown and Solar, 1998; Brown, 2007). Migmatites, which are weak crustal material as long as they are kept at high temperature, are the source of magmas that concentrate within plutons of various sizes. On the other hand, interactions between magmatism and lithospheric deformation, and more specifically interactions of plutons with crustal-scale tectonics, depend first of all upon the rate of magma production and, to a second order, strain rates. The rate of magma transfer to the crust is indeed so large compared to tectonic strain rates that the construction of plutons is thought in a first approach to be little influenced by the tectonic setting, especially when small plutons are concerned (de Saint Blanquat et al., 2011).
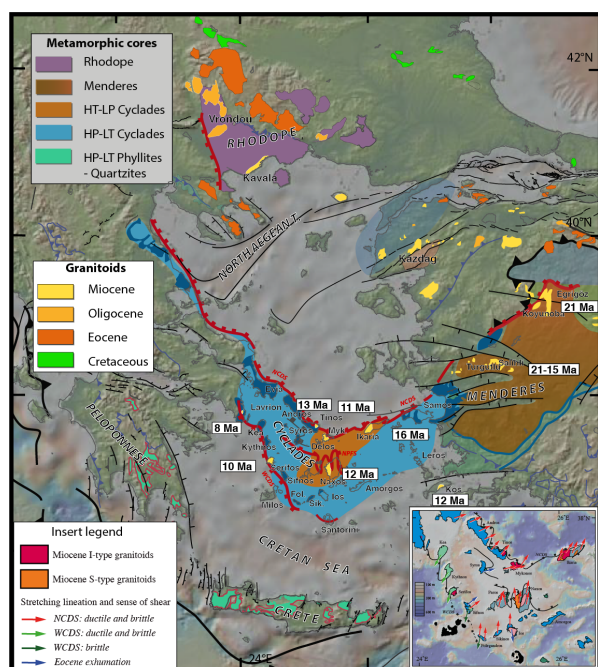

Figure 1: Tectonic map of the Aegean region showing the successive generations of granitoids since the late Cretaceous. Modified from Jolivet et al. (2015).

The Miocene Aegean plutons (figure 1), emplaced in an extensional context within metamorphic core complexes (MCCs), may however depart from this behaviour. Despite a moderate volume, they have indeed recorded the complete evolution from syn-tectonic magmatic flow to localized mylonitic deformation along the main detachment (Faure and Bonneau, 1988; Urai et al., 1990; Faure et al., 1991; Lee and Lister, 1992; Gautier et al., 1993;

54   Laurent et al., 2015; Rabillard et al., 2015; Bessière et al., 2017; Rabillard et al., 2018). All of

55   them moreover show a systematic magmatic and tectonic evolution of the host MCCs with

56   several magmatic pulses and a series of detachments forming sequentially during exhumation

57   (Rabillard et al., 2018). Several of them also show an association of mixed or mingled felsic

58   and mafic magmas, with an evolution from a significant component of crustal melting toward

59   more mafic composition, a trend that is common in post-orogenic magmas (Bonin, 2004).
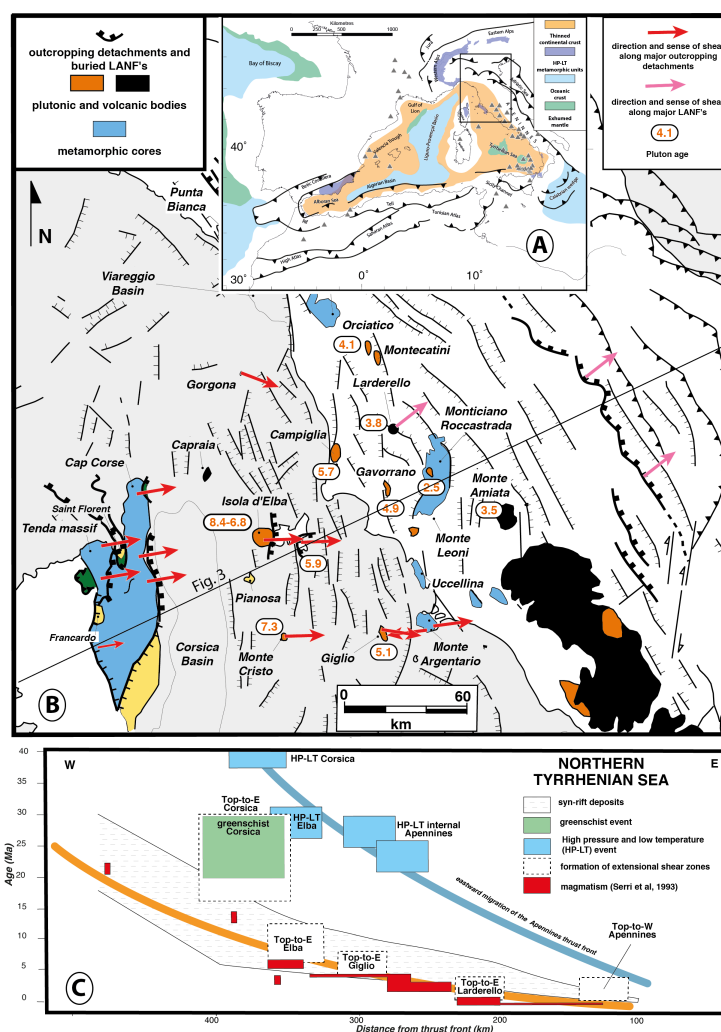
60

61   *Figure 2: Tectonic map of the Central and Western Mediterranean with the distribution of*
62   *recent magmatism (Savelli, 1988; Serri et al., 1993; Savelli, 2002b, a; Duggen et al., 2005;*
63   *Avanzinelli et al., 2009; Savelli, 2015). Tectonic map (B) of the northern Tyrrhenian region*
64   *and Northern Apennines and (C) a diagram showing the evolution of the ages of syn-rift basins,*
65   *metamorphic events and magmatism along a cross-section from Corsica to the Apennines,*
66   *modified from Jolivet et al. (1998).*

3

67

68   Whether these features are characteristic of syn-extension plutons in post-orogenic back-arc

69   environments is the question we address in this paper, through a comparison of the Aegean

70   plutons with those of the northern Tyrrhenian Sea and Tuscany, with a focus on Elba Island in

71   the Tuscan archipelago (figure 2). Striking similarities can indeed be observed between the two

72   contexts in terms of tectonic and magmatic evolution. We propose and test a scenario of

73   formation and emplacement of plutons in a back-arc post-orogenic context below crustal-scale

74   detachments.

2. Geodynamic context

76   The Aegean and North Tyrrhenian granitoids were emplaced during the Miocene and part

77   of the early Pliocene in the back-arc regions of the Hellenic and Apennines subduction,

78   respectively (Serri et al., 1993; Jolivet et al., 1998; Pe-Piper and Piper, 2002, 2007; Avanzinelli

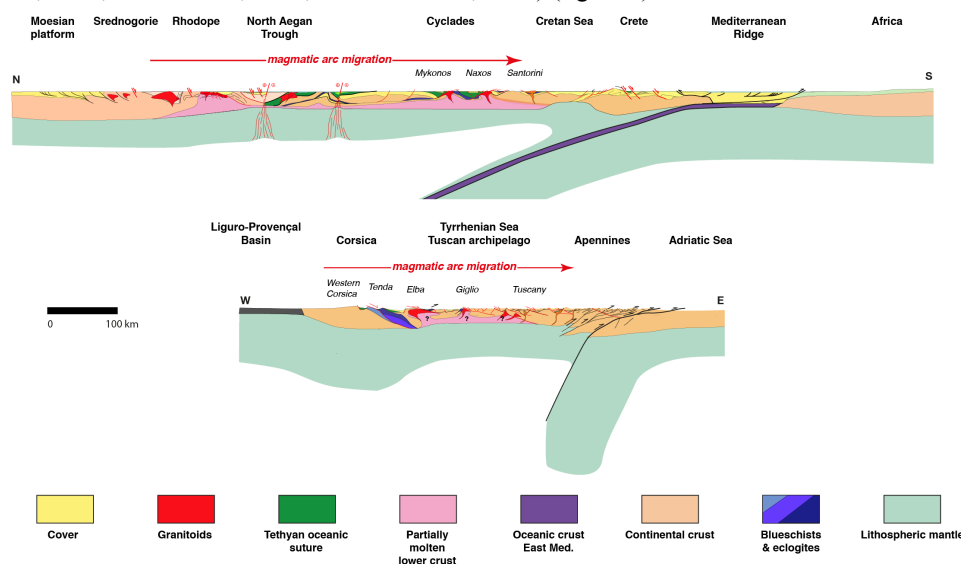79   et al., 2009; Jolivet et al., 2015; Rabillard et al., 2018) (figure 3).

80

81   *Figure 3: Two lithospheric-scale cross-sections of the Aegean domain (Jolivet and Brun,*
82   *2010) and the Northern Tyrrhenian Sea and the Apennines (Jolivet et al., 1998).*

83

84   These two subduction zones started to retreat approximately at the same time, 30-35 Ma

85   ago (Jolivet and Faccenna, 2000). A first-order change in the geodynamics of this region indeed

86   occurred at this period, also coeval with the hard collision between Africa and Eurasia in the

87   eastern and westernmost Mediterranean. The subducting African lithosphere, locked between

88   two collision zones, continued to subduct northward but with a significant component of retreat.

89   Since that time subduction has been continuous, with however several episodes of slab

90   detachment and tearing (Wortel and Spakman, 2000; Spakman and Wortel, 2004; Faccenna and

91   Becker, 2010; Faccenna et al., 2014). The Aegean plutons studied in this paper were emplaced

92   during the formation of a large tear in the subducting lithosphere between 16 and 8 Ma (Jolivet

93   et al., 2015). The oldest North Tyrrhenian pluton is dated around 7 Ma in Elba (Westerman et

94   al., 2004) and the youngest ones, Pliocene in age (Serri et al., 1993), are currently exploited for

95   geothermal energy in Tuscany (Rossetti et al., 2008; Rochira et al., 2018). All these plutons

96   contain a significant component of crustal melts and some of them are linked with migmatite

97   domes such as on Naxos, Mykonos and Ikaria (Jansen, 1977; Urai et al., 1990; Denèle et al.,

98   2011; Beaudoin et al., 2015; Vanderhaeghe et al., 2018). Mixing and mingling with mafic

99   magmas are also observed in some of these plutons and the general evolution shows an increase

100   of the mantle component with time.

101   Most of these plutons are associated with low-angle normal faults (LANF) and shear

102   zones and they were emplaced in the core of MCCs (Faure et al., 1991; Lee and Lister, 1992;

103   Lister and Baldwin, 1993; Daniel and Jolivet, 1995; Jolivet et al., 1998; Berger et al., 2013;

104   Bessière et al., 2017; Rabillard et al., 2018). These LANF and associated ductile shear zones

105   (we use the term "detachment" for the whole structure, brittle and ductile) started to form before

106   the emplacement of the plutons, in both regions. The main difference between the two regions

107   are the kinematics of these detachments (figure 3) (Jolivet et al., 2008) and the role of tectonic

108   inheritance. In the Aegean, most of the MCCs are capped by north-dipping detachments except

109   in the southwest where south-dipping detachments are observed. The north-dipping

110   detachments probably partly reactivate former thrusts related to the building of the Hellenides

111   orogenic wedge. In the Northern Tyrrhenian Sea and in Tuscany, all detachments dip eastward,

112   i.e. toward the subduction zone. In that case, the detachments cannot reactivate the former

113   thrusts of the internal Apennines that dip westward. Only in the case of the oldest detachments,

114   found in Alpine Corsica, can they correspond to reactivated thrusts. The case of Elba Island

115   shows the detachments cutting down-section eastward within the stack of former nappes (Keller

116   and Pialli, 1990; Collettini and Holdsworth, 2004). Whatever the nature (i.e. reactivated

117   structure or not) and the sense of shear of these detachments, the interaction with the plutons

118   follows a similar pattern that we recall below, first briefly for the Aegean region and then for

119   Elba Island (see Rabillard et al., 2018, for details on the Aegean).

120

3. Aegean plutons

The Miocene Aegean and Menderes plutons were emplaced during a short time period between ~20 Ma and 8 Ma, the oldest cropping out in the Menderes massif and the youngest in the western part of the Aegean region (figures 1, 3) (Jolivet et al., 2015). Those occupying the Cycladic domain are all associated with detachments, either north or south-dipping (figure 4) (Grasemann and Petrakakis, 2007; Rabillard et al., 2018).
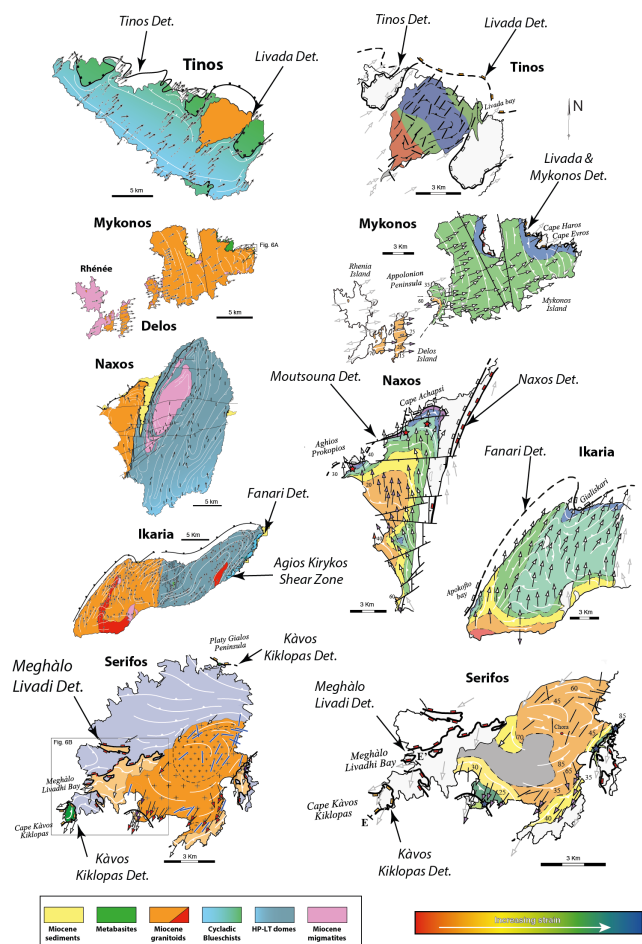

Figure 4: Five examples of the Aegean granitoids showing the interactions between deformation and intrusion, after Rabillard et al. (2018) and references therein. The left column show maps of the entire islands and the right column shows the internal fabrics of the plutons. These maps were obtained based on deformation grades observed in the field, a scale of grades was designed for each pluton to describe the gradients. Arrows show stretching lineations and sense of shear and black bars on the Tinos and Serifos plutons shows the direction of the magnetic lineation.

6

136

Except for Serifos and Lavrion plutons, associated with the West Cycladic Detachment System (WCDS) (Grasemann and Petrakakis, 2007; Berger et al., 2013; Scheffer et al., 2016), the plutons crop out in the core of MCCs exhumed by north-dipping detachments, such as the North Cycladic Detachment System (NCDS) (Gautier and Brun, 1994b, a; Jolivet et al., 2010) or the Naxos-Paros Fault System (NPFS) (Urai et al., 1990; Gautier et al., 1993; Vanderhaeghe, 2004; Bargnesi et al., 2013; Cao et al., 2017). The detachments upper plate is made of the Upper Cycladic Nappe, a remnant of the Pelagonian domain, made of greenschists-facies metabasites or serpentinite with, in a few cases, early to late Miocene sediments deposited during extension (Angelier et al., 1978; Sanchez-Gomez et al., 2002; Kuhlemann et al., 2004; Menant et al., 2013). The MCCs are made of various units of the Cycladic Blueschists, more or less retrograded in the greenschist-facies, or the Cycladic basement, showing HT-LP metamorphic facies and even anatectic conditions on several islands, such as Naxos, Paros, Mykonos or Ikaria (Buick and Holland, 1989; Urai et al., 1990; Buick, 1991; Keay et al., 2001; Duchêne et al., 2006; Seward et al., 2009; Kruckenberg et al., 2011; Beaudoin et al., 2015; Laurent et al., 2015; Rabillard et al., 2015; 2018). The plutons intruded these MCCs and were sheared at the top by the detachments during their emplacement (Rabillard et al., 2018).

The granitoids show a variety of facies and composition, but most of them have a crustal melting component and some are closely associated with migmatites, as on Ikaria or Mykonos (Vanderhaeghe, 2009; Kruckenberg et al., 2011; Denèle et al., 2011; Beaudoin et al., 2015; Jolivet et al., 2021). Compositions show a common trend for these plutons indicating that they crystallized primarily from I-type magmas with some contamination by the continental crust and little fractionation (figure A1, Appendix A). Field evidence show a close association of these I-type intrusions with two-micas granites (in Ikaria for instance), migmatites, or both (Ikaria, Naxos, Paros, Rheneia-Delos) (Pe-Piper et al., 1997; Pe-Piper, 2000; Pe-Piper et al., 2002; Vanderhaeghe, 2004; Bolhar et al., 2010; Bolhar et al., 2012; Bargnesi et al., 2013; Beaudoin et al., 2015; Laurent et al., 2015; Jolivet et al., 2021). Tinos, Ikaria and Serifos granitoids were emplaced in several magma batches with an evolution through time, characterized by more and more mafic compositions and a decrease of the grain size (Grasemann and Petrakakis, 2007; Ring, 2007; Bolhar et al., 2010; Petrakakis et al., 2010; de Saint Blanquat et al., 2011; Bolhar et al., 2012; Beaudoin et al., 2015; Laurent et al., 2015; Rabillard et al., 2015; Ducoux et al., 2016). On Serifos and Naxos, the farthest parts of the pluton from the detachment show an enrichment in mafic enclaves and evidence for magma

169   mixing and mingling in the roots of the rising plutons (Rabillard et al., 2015; Bessière et al.,

170   2017; Rabillard et al., 2018).

171   A common evolution is observed in several of these plutons during their interaction with

172   the system of detachments exhuming their host MCC (Rabillard et al., 2018). A series of two

173   or three detachments is observed (figure 4, figure 5).

174
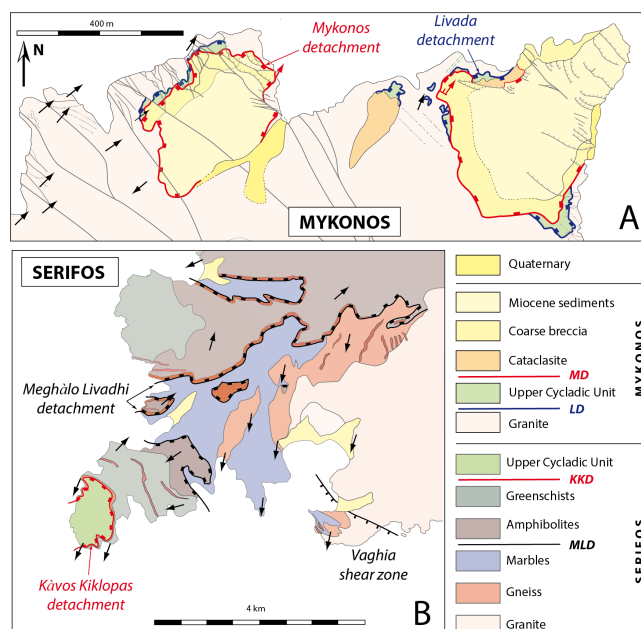
*Figure 5: Details of the two detachments on Mykonos and Serifos. A: northeastern Mykonos
(see location on figure 5), B: Southwest Serifos. The Mykonos (MD) and Livada (LD)
detachments on Mykonos and the mineralized veins and normal faults (baryte and iron-
hydroxides) – grey- are after Menant et al. (2013). The Kàvos Kiklopas (KKD) and Meghàlo
Livadi (MLD) detachments on Serifos are after Grasemann and Petrakakis (2007) and
Ducoux et al. (2016).*

181

182   The deepest one is mostly ductile and has started to act long before the granitic intrusion

183   that ultimately intrudes it. The upper detachments are mostly brittle and are locally intruded by

184   dykes and sills emanating from the main pluton. When a sedimentary basin is present, it is

185   deposited on top of the uppermost detachment during extension and can be partly affected by

186   mineralized veins (Menant et al., 2013). All plutons show a gradient of shearing deformation

187   toward the detachment with an evolution from ductile to brittle (Figure 4). The maps shown in

188   figure 4 were drawn after detailed field observations and the construction of a scale of up to 7

189   grades of progressive deformation, from non-deformed granitic texture to ultra-mylonites, with

190   the progressive appearance of foliation, stretching lineation, localization of C and C' shear

191 bands (Berthé et al., 1979; Lister and Snoke, 1984), for details see Rabillard et al. (2018). The
192 inner parts of the plutons show mixing of acidic and mafic magmas and a co-magmatic
193 deformation, co-axial with the post-solidus deformation along the detachment (Rabillard et al.,
194 2015; 2018). The flow of magma is thus oriented by the regional strain field. Serifos shows (i)
195 a decrease of grain size through time with an inner facies with smaller grain size and finally
196 fine-grained dykes and (ii) evidence for hydrothermalism in the root zone of the pluton,
197 suggesting that the magmatic system was open upward with a possible volcano-plutonic system
198 (Rabillard et al., 2015; 2018).

199

4. North Tyrrhenian plutons

201

202 The Monte Capanne pluton on Elba island (figure 6) is the oldest of a series of plutons
203 cropping out in the Tuscan archipelago and onshore Tuscany (Serri et al., 1993; Westerman et
204 al., 2004; Avanzinelli et al., 2009).
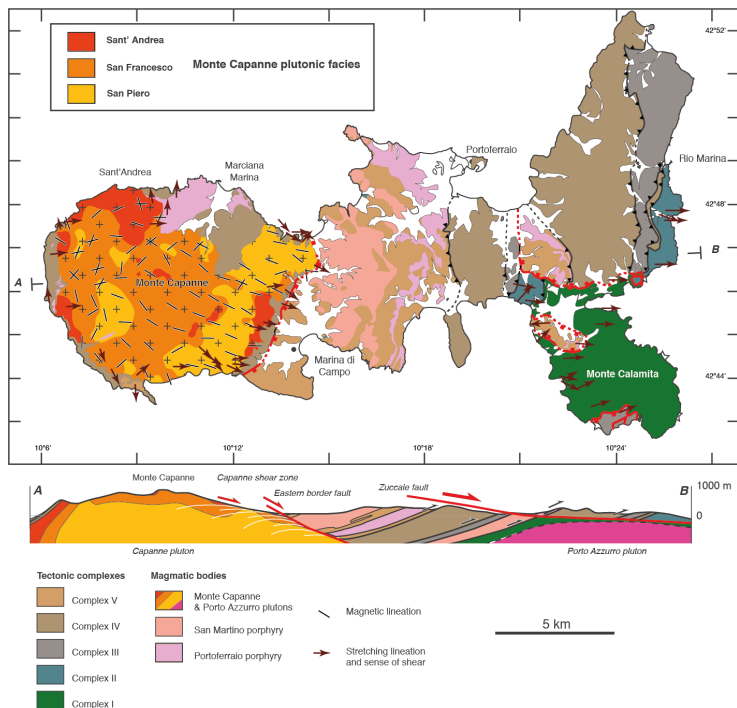
205

206 *Figure 6: Tectonic map and cross-section of Elba Island showing the main tectonic units and*
207 *the main extensional shear zones and detachments, modified after Bianco et al. (2015).*
208 *Details of the internal structure of the Monte Capanne intrusions are reported based on*
209 *Farina et al. (2010).*

9

210

211   These plutons belong to magmas migrating from west to east between the end of the

212   Oligocene and the Quaternary, mimicking the migration of the Apennines thrust system and the

213   HP-LT metamorphism of the internal Apennines and Tuscan Archipelago (Serri et al., 1993;

214   Jolivet et al., 1998) (figure 2). This situation is thus very similar to the Aegean Sea. The

215   decrease of the time lag between the recording of HP-LT metamorphism or the activation age

216   of the thrust front and the magmatism has been interpreted as a consequence of slab steepening

217   during retreat (Jolivet et al., 1998; Brunet et al., 2000). Pluton ages decrease eastward from ~8

218   Ma to 2-3 Ma (figure 2). Among the youngest plutons are those powering the active geothermal

219   fields of Larderello and Monte Amiata (Camelli et al., 1993; Brogi et al., 2003; Rossetti et al.,

220   2008). The oldest plutons are observed offshore on Elba (Monte Capanne and Porto Azzuro

221   plutons), Monte Cristo and Giglio islands (Westerman et al., 1993) (figure 2). These four

222   plutons are granodiorites/monzogranites and they all display a contamination with crustal

223   magmas with a main source thought to be lower crustal anatexis (Serri et al., 1993; Innocenti

224   et al., 1997). They were emplaced within an overall extensional context during the rifting of the

225   Northern Tyrrhenian Sea in the back-arc region of the Apennines (Jolivet et al., 1998). First

226   evidenced in Alpine Corsica and on Elba island, a series of east-dipping low-angle detachments

227   controlled the kinematics of extension along the Corsica-Apennines transect from the

228   Oligocene onward (Jolivet et al., 1998). Extension is shown to migrate from west to east with

229   time and it is active at present in the highest altitude regions of the Apennines just west of Corno

230   Grande peak with however west-dipping normal faults (D'Agostino et al., 1998). The youngest

231   east-dipping low-angle normal faults are seismically active in the Alto Tiberina region

232   (Collettini and Barchi, 2002, 2004; Pauselli and Ranalli, 2017). Evidence for top-to-the east

233   shearing deformation is found within the plutons of the Tuscan archipelago, but the

234   detachments crop out nicely mostly on Elba island (Keller and Pialli, 1990; Daniel and Jolivet,

235   1995; Collettini and Holdsworth, 2004; Liotta et al., 2015).

236

237   ***4.1. Monte Capanne pluton, Elba Island***

238   Elba, the largest island of the Tuscan archipelago, shows the relations between

239   peraluminous magmatic bodies and two east-dipping low-angle shear zones cutting down-

240   section within the Tuscan nappe stack emplaced before extension started (figure 6) (Keller and

241   Pialli, 1990; Bouillin et al., 1993; Pertusati et al., 1993; Daniel and Jolivet, 1995; Westerman

242   et al., 2004; Bianco et al., 2015). Five thrust packages (complexes I to V) are separated by west-

243   dipping low-angle reverse faults (Trevisan, 1950; Barberi et al., 1967; Perrin, 1975; Pertusati

244 et al., 1993; Bianco et al., 2015; Bianco et al., 2019). Long thought free of any HP-LT imprint,

245 at variance with the nearby Gorgona and Giglio islands where the presence of Fe-Mg-carpholite

246 attest for blueschist-facies metamorphism (Rossetti et al., 1999a; 1999b), the nappe stack has

247 only recently revealed HP-LT parageneses along the east coast of the island (Bianco et al.,

248 2015). Through a correlation with the HP-LT units of Gorgona (Rossetti et al., 1999), where

249 ^{40}Ar/^{39}Ar dating on micas yielded ages around 25 Ma (Brunet et al., 2000), the Elba blueschists

250 are attributed to the Oligocene-Early Miocene.

251   The Nappe stack is intruded by the shallow-level San Martino and Portoferraio porphyries

252 coeval with the Monte Capanne pluton (figure 6), spanning a short period between 8 and 6.8

253 Ma, showing that the magma has intruded the detachment in a late stage (Saupé et al., 1982;

254 Juteau et al., 1984; Ferrara and Tonarini, 1985; Bouillin et al., 1994; Westerman et al., 2004).

255 The Monte Capanne intrusion makes the major part of the western half of the island and the

256 highest peak. It is surrounded by a contact metamorphic aureole developed at the expense of

257 the nappe stack (Duranti et al., 1992; Dini et al., 2002; Rossetti et al., 2007; Rossetti and Tecce,

258 2008). The metamorphic parageneses within the aureole suggest an emplacement at a depth of

259 4-5 km (Dini et al., 2002; Rocchi et al., 2002; Farina et al., 2010; Pandeli et al., 2018). The

260 pluton shows an internal deformation with a gradient of shearing toward the east attested by the

261 magnetic fabric, stretching lineation and sense of shear (Bouillin et al., 1993; Daniel and Jolivet,

262 1995). The pluton and the metamorphic aureole are separated from the nappe stack by an east-

263 dipping low-angle shear zone (Capanne shear zone) evolving into a brittle east-dipping fault

264 (eastern border fault) (Daniel and Jolivet, 1995). Syn-kinematic contact metamorphism

265 minerals coeval with top-to-the east kinematic indicators attest for the syn-kinematic nature of

266 the intrusion (Daniel and Jolivet, 1995; Pandeli et al., 2018).

267   The eastern part of the island shows granitic dykes emanating from the buried younger

268 Porto Azzuro pluton intruding the Calamiti schists complex (Complex I, figure 6) (Daniel and

269 Jolivet, 1995; Maineri et al., 2003; Musumeci and Vaselli, 2012). Here too, evidence for top-

270 to-the east shearing at the time of intrusion have been described (Daniel and Jolivet, 1995)

271 (figure 7). The pluton and the Calamiti schists are topped by the Zuccale low-angle normal fault

272 that cuts down-section across the entire nappe stack with clear evidence of top-to-the east

273 shearing (figure 8) (Keller and Pialli, 1990; Keller et al., 1994; Collettini and Holdsworth,

274 2004).

275   The main facies of the Monte Capanne pluton exhibits a constant, peraluminous,

276 monzogranitic composition (Poli et al., 1989; Dini et al., 2002; Gagnevin et al., 2004) while the

277 mafic microgranular enclaves (MME) varies from tonalitic-granodioritic to monzogranitic. The

278   leucogranitic dykes are syenogranitic in composition (Gagnevin et al., 2004). Gagnevin et al.

279   (2004) proposed a multiphase magmatic emplacement from peraluminous magmas issued from

280   melting of a metasedimentary basement and hybridized with mantle-derived mafic magmas

281   whose heat supply possibly enhanced wall-rock assimilation. In addition, injection of mantle-

282   derived magma in the Sant' Andreas facies would have triggered extensive fractionation and

283   mixing of the basic magma with the resident monzogranitic mush (Poli and Tommasini, 1991).
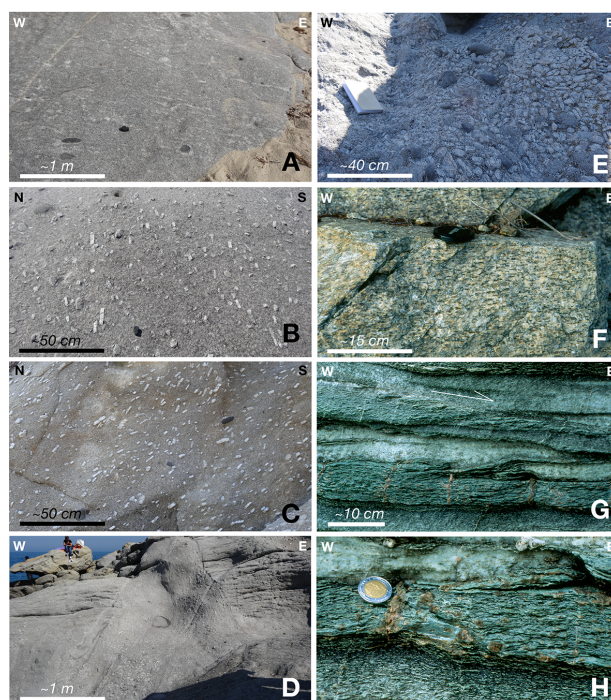
284

285   *Figure 7: Photographs of the Sant' Andrea facies in the Monte Capanne pluton and of the*
286   *deformation along the eastern margin of the pluton, in the pluton itself and in the contact*
287   *metamorphic aureole. A: general view of the orientation of K-feldspar megacrysts and some*
288   *mafic enclaves. B: Detailed view of the oriented K-feldspar megacrysts (horizontal plane). C:*
289   *zoom on the orientation of K-feldspar megacrysts (vertical plane). D: Cotoncello dyke. E:*
290   *cluster of K-feldspar megacrysts in the vicinity of the Cotoncello dyke. F: Mylonitic foliation*
291   *within the Monte Capanne shear zone. G: Sigmoidal foliation and top-to-the-east sense of*
292   *shear within the metamorphic aureole of the Monte Capanne pluton. H: detailed view of syn-*
293   *kinematic contact metamorphism garnets in veins perpendicular to the regional stretching*
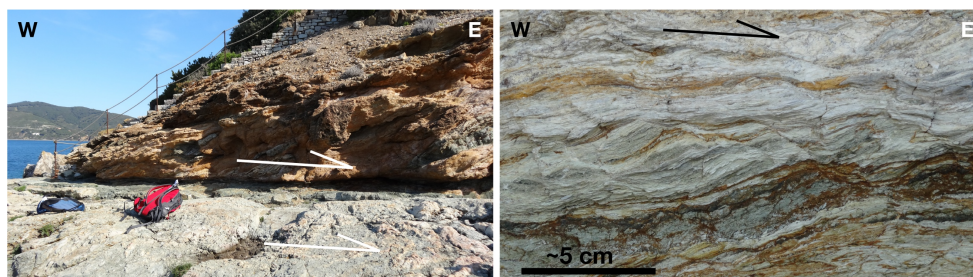294   *direction.*

295

Solid Earth
Discussions

Open Access

EGU

296

297 *Figure 8: Photographs of the Zuccale detachment and its internal structure (see Collettini*
298 *and Holdsworth, 2004). Upper: overview of the detachment fault. Lower left: Detail of the*
299 *contact zone and the truncated foliation in the hanging wall. Lower right: detail of the shear*
300 *bands indicating top-to-the east kinematics.*

301

302 The internal magmatic structure of Monte Capanne pluton has been described based on the
303 abundance of large alkali-feldspar phenocrysts (Farina et al., 2010). Three main facies
304 corresponding to different magma batches emplaced within a too short period to be
305 discriminated based on geochronology are reported with downward fining of grain size (figure
306 6). The largest grain size characterizes the upper Sant' Andrea facies that mainly crops out in
307 the northwest of the pluton, while the finest grain size is observed in the lower San Piero facies
308 cropping out mainly in its eastern part, within the zone affected by the most intense shearing.
309 These three facies delineate an asymmetric dome-shaped bulk structure compatible with the
310 general top-to-the east sense of shear. In the westernmost part of the Monte Capanne pluton
311 near Sant' Andrea, mafic products are observed as large enclaves, with evidence of magma
312 mixing and mingling. These mafic enclaves are mostly found in the Sant' Andrea facies that
313 was emplaced first. Their occurrence in the westernmost part of the plutonic body, the farthest
314 from the detachment, with a geometry similar to that observed on Serifos island in the Cyclades
315 (Rabillard et al., 2015), suggests that they are associated with the root of the pluton.

316 Assuming that the three main felsic facies correspond to three successive intrusion
317 batches, one observes an evolution toward finer grain size through time, an evolution that is
318 compatible with progressive exhumation and also with a shorter residence time in the magma
319 chamber, suggesting opening of the magmatic plumbing toward the surface leading to volcanic
320 activity, as recorded above the detachment. The last episodes of intrusive activity are seen as a
321 series of felsic dykes striking N-S or NE-SW, due to eastward extensional brittle deformation
322 while the pluton was at near solidus conditions.

323

324 ***4.2. Orientation of K-feldpar megacrysts***

325   A detailed study of the orientation of feldspar megacrysts was conducted along the shore

326   near Sant'Andrea (figures 7, 9, 10, 11). The pluton is there characterized by a high

327   concentration of megacrysts and of mafic enclaves reaching several meters in size. Megacrysts

328   show euhedral shapes in general.
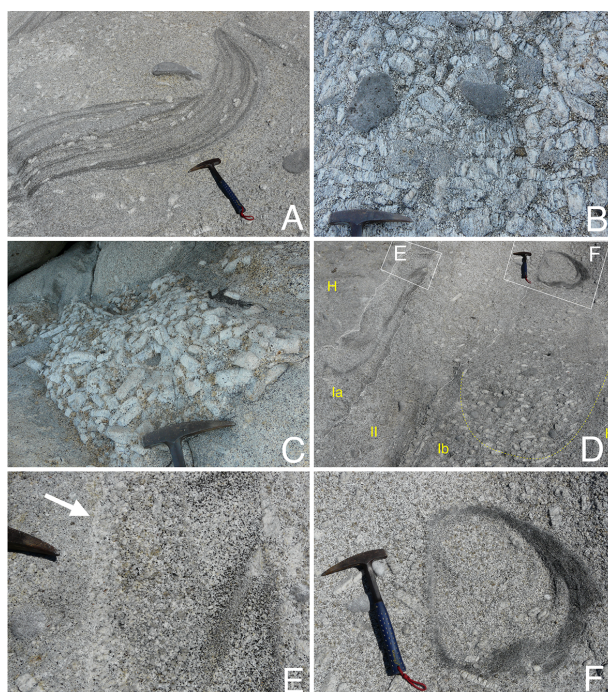
329

330   *Figure 9: Photographs of the root zone of the Sant'Andrea facies in the melange zone in and*
331   *around the Cotoncello dyke. A: Schlieren with cross-bedding. B: Mush zone with cluster of*
332   *K-feldspar megacrysts and mafic enclaves. C: Isolated blob of mush zone with large K-*
333   *feldspar megacrysts. D: Folded alternation of leucocratic and melanocratic layers with*
334   *schlierens. E: Detail of D, schlieren. F: detail of D: schlieren tube.*

335

336   Although the orientation of megacrysts is quite stable at the scale of a few hundred meters,

337   in the westernmost region the presence of the large enclaves is associated with a disorientation

338   of the megacrysts (figure 10A), indicating increasing tortuosity of the flow wrapping around

339   them associated with local turbulence in pressure shadows. Smaller enclaves are in general

340   aligned with the megacrysts. Some of the mafic enclaves with lobate shapes show a sharp

341   boundary with the felsic matrix, suggesting quenching of a hot mafic magma within the cooler

342   felsic magma (Fernandez and Barbarin, 1991; van der Laan and Wyllie, 1993; Fernandez and
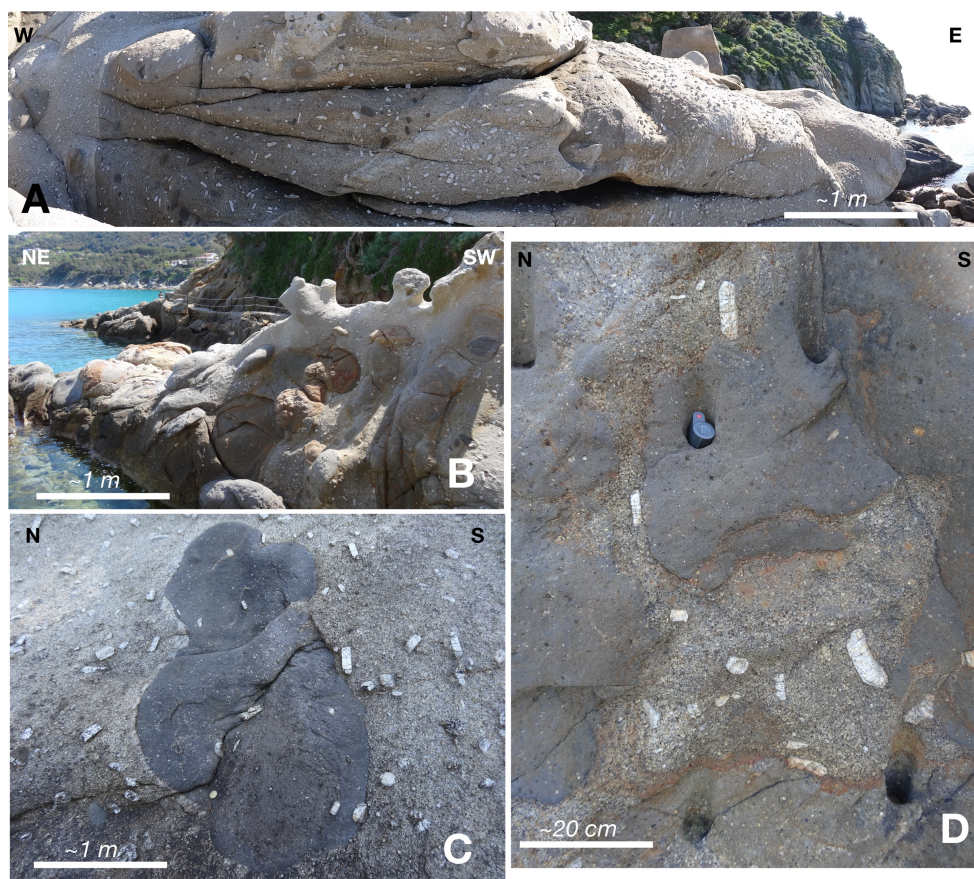
343   Gasquet, 1994).

344

14

Figure 10: *Photographs of large mafic enclaves and melange zones in the westernmost part of the Sant'Andrea facies showing the disorientation of K-feldspar megacrysts and melange facies (mingling).*

Other enclaves are less mafic and show evidence of magma mingling-mixing. The disaggregation process of the mafic magma responsible of theses enclaves could happened either in a deep-seated magmatic chamber (Christofides et al., 2007), or more likely in the ascent conduit as a result of remelting of chilled mafic margins (Fernández and Castro, 2018) and subsequent viscous fingering dynamics (Perugini et al., 2005). Megacrysts contain inclusions of biotite, plagioclase and quartz and show euhedral shapes in general, although resorption surface has been noticed (Gagnevin et al., 2008). Other enclaves are less mafic and show evidence of magma mingling-mixing. These enclaves are associated with an aureole where feldspar crystals are concentrated, showing that the assimilation of the enclave occurred at the magmatic stage. Megacrysts are sometimes included within the mafic enclaves, showing that they were already present before the solidification of enclaves and thus providing evidence

361   of low viscosity contrast between the enclaves and the host magma at the magmatic stage. All

362   these observations suggest that this western zone is a mixing between a mafic magma of mantle

363   origin and a felsic magma partly issued from crustal anatexy and that this part of the pluton is

364   close to the main feeder. This conclusion is confirmed by AMS (anisotropy of magnetic

365   susceptibility) showing that the magnetic foliation and lineation are steeper there than anywhere

366   else in the pluton (Bouillin et al., 1993).
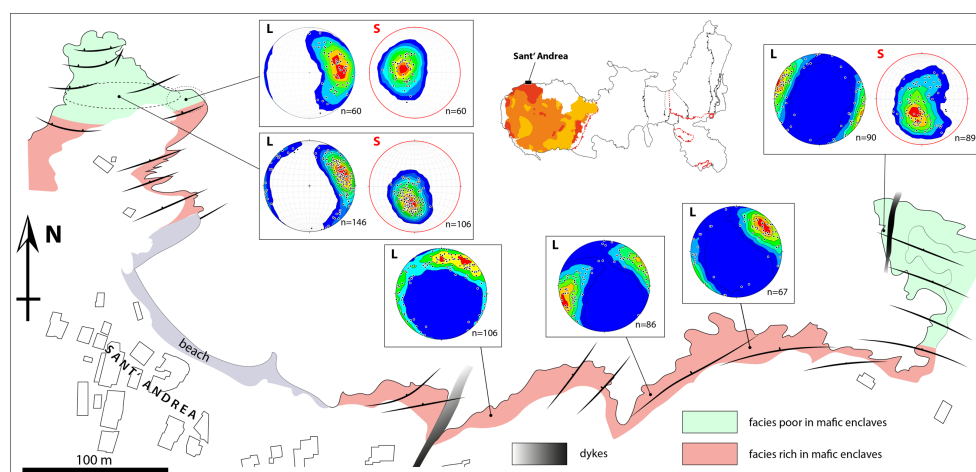
367

368   *Figure 11: Detailed study of the orientation of K-feldspar megacrysts in the Sant-Andrea*
369   *facies with foliation trajectories.*
370

371   Further to the east, still within the Sant' Andrea facies, the main granite is intruded by a

372   N-S syeno-granitic dyke-like structure near Cotoncello headland, made of a finer-grained facies

373   and a lower concentration of megacrysts and enclaves (figure 7D, figure 9). In its vicinity, the

374   host granite contains folded schlierens with cross-bedding (Figure 9A). Within these large

375   schlierens, the megacrysts are aligned parallel with the folded foliation of biotite-rich layers.

376   From place to place, decametric megacryst-rich mush zones enriched in decametric and

377   rounded mafic enclaves occur in this host facies (Figure 9B). In addition, isolated blobs of

378   mush, characterized by an irregular shape, are observed in the coarse-grained, megacryst-poor

379   domains (Figure 9C). These blobs originate from the disruption of preexisting mush zones

380   within the root zone by subsequent magma injection as illustrated by the dyke-like structure

381   (Rodríguez and Castro, 2019). This structure is composed of three successive injections

382   characterized by undulating and fuzzy boundaries (Figure 9D). The westernmost injection

383   (injection Ia, figure 9D) shows folded alternating leucocratic flow-sorted layers made of quartz,

384   K-feldspar and plagioclase with more melanocratic layers rich in biotite that can be described

385   as schlierens (Figure 9E). These schlierens are folded and cross-cut by a subsequent and final

386　injection (Figure 9D, injection II). In the easternmost injection (Figure 9D, injection Ib), K-

387　feldspar megacrysts are accumulated and their orientation defines a concave upwards foliation.

388　Such mineral fabric is similar to those described by Rocher et al. (2018) in finger and drip

389　structures developed at the margins of the Asha pluton (NW Argentina) and interpreted as

390　mechanical accumulation in a downward localized multiphase magmatic flow. In addition, this

391　megacrysts accumulation is associated at its top with ring schlieren that could represent a cross-

392　section of a schlieren tube (e.g. Žák and Klomínský, 2007) (figure 9F). Ring schlierens are also

393　associated with drip structures in the Asha pluton among others (Paterson, 2009; Rocher et al.,

394　2018). The most external rim between the host body H and injection Ia (Figure 9D) is associated

395　with a reaction zone with recrystallization of quartz and K-felspar (Figure 9E, white arrow).

396　Outside the injections, the mineral fabric shown by the K-feldspar megacrysts tends to

397　reorientate parallel to the rims.

398　　　All these observations point out to an injection of a low viscosity, crystal poor, magma

399　with a viscosity contrast of about one order of magnitude lower with respect to its host magma

400　(Wiebe et al., 2017). Mineral fabrics and accumulation, folded and ring schlieren indicate that

401　the structures were formed by localized multiphase magmatic flow when the crystallizing host

402　magma remained partially molten, probably containing around 50% of crystals (Weinberg et

403　al., 2001). The Cotoncello dyke-like structure is thus co-magmatic with the Sant'Andrea facies,

404　but the pluton was already enough crystallized to allow the formation of N-S cracks in the

405　crystal mush capable of transmitting tectonic stress where the magma was injected.

406　　　Between the Cotoncello dyke and the root zone to the west, the proportion of enclaves

407　and megacrysts is everywhere high. Systematic measurements of felspar megacrysts were made

408　(figure 11). Mineral foliation and lineation represents the main orientation distributions of the

409　orientation of (010) faces and [001] major axis of the measured crystals, respectively. At the

410　scale of a few hundred meters the fabric shows a consistent pattern with a low-angle north-

411　dipping foliation more prominent in regions poorer in mafic enclaves. The lineation is in

412　average E-W trending. Late mafic and acidic dykes strike perpendicular to the lineation. Within

413　the mélange zone, the mineral fabric is often perturbated approaching enclave swarms. Then,

414　the fabric becomes more uniform with variations around an average ENE-WSW trend from

415　N30 to N100°E for the long axes of megacrysts.

416　　　As the megacrysts were formed in early magmatic conditions (Vernon, 1986; Vernon and

417　Paterson, 2008), they were in suspension within the melt. Such a preferential orientation is due

418　to a rigid rotation of isolated crystals within a viscous matrix submitted to magmatic flow

419　(Fernandez and Laporte, 1984). In the present case, the various observations attesting for a co-

17

420 magmatic fabric show that the preferential orientation of the megacrysts foliation results from

421 a fossilization of the magmatic flow. The large-scale variations of the foliation attitude suggest

422 in addition that the E-W to ENE-WSW flow was laminar in general, except in the immediate

423 vicinity of the large enclaves where the flow wrapping around these stronger bodies was more

424 turbulent.

425   These detailed observations show that the internal magmatic fabric of the pluton is similar

426 in orientation with its overall tectonic fabric, including the sub-solidus deformation along the

427 eastern margin due to the detachment with a main stretching direction oriented WNW-ESE, as

428 shown by magnetic susceptibility studies (Bouillin et al., 1993) and deformation features near

429 the main eastern contact within the eastern extensional shear zone (Daniel and Jolivet, 1995).

430 This focussing of the pluton fabric, from the magmatic stage to the brittle stage around an E-W

431 stretching direction compatible with the extensional shear along the main detachment, suggests

432 that the magmatic flow was oriented parallel to the main direction of extension active at crustal

433 scale since the magmatic stage. A continuum is thus observed from the magmatic stage to the

434 sub-solidus deformation and the localization of the detachment, and this continues during the

435 emplacement of the younger Porto-Azzuro pluton and the formation of the Zuccale low-angle

436 normal fault. This evolution recalls that of the Aegean plutons summarized above.

437

5. Discussion and modelling

439

5.1.   Synthesis of observations

441

442   The coaxiality of the structures measured in the Monte Capanne pluton from its magmatic

443 stage to the tectonic overprint is similar to observations made on the Cycladic plutons,

444 especially Ikaria and Serifos where a similar gradual transition is observed from the magmatic

445 stage to the localisation of strain along the main detachment. The similarity goes further as the

446 root of the pluton shows a mixture of mafic and felsic facies. On Serifos (figure 4), field

447 observations show that the root of the pluton is characterized by vertical or steep dykes and

448 some of them are dilacerated by the top-south flow while the magma is still viscous (Rabillard

449 et al., 2015). Moving toward the detachment, the sub-solidus deformation takes over with a N-

450 S trending stretching lineation and top-south kinematic indicators. A similar evolution can be

451 observed in the Raches pluton of Ikaria island in the Cyclades (Laurent et al., 2015). Emplaced

452 below to top-to-the north detachment, the magma shows a steep foliation in the south far from

453   the detachment and it flattens toward the north to become parallel to the detachment plane.

454   Evidence of co-magmatic stretching and shearing parallel to the regional stretching direction is

455   observed in the southern side of the pluton and sub-solidus mylonitization and ultra-mylonites

456   on the northern side. A similar situation can be described in the case of the Naxos granodiorite

457   (Bessière et al., 2017). All cases show the syn-kinematic character of the pluton, the best

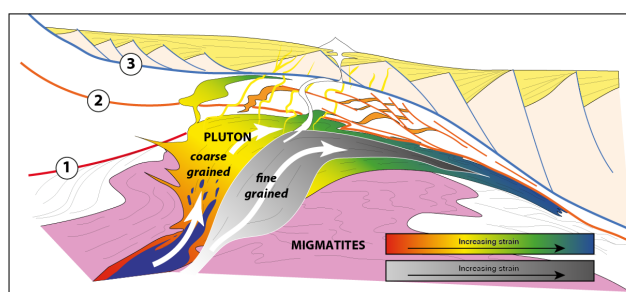458   evidence being the syn-kinematic contact metamorphism.

459

460   *Figure 12: Schematic section showing a conceptual model of the relations between syn-*
461   *kinematic plutons and the detachments, based on the examples of the Aegean and North*
462   *Tyrrhenian plutons. Modified from Rabillard et al. (2018).*

463

464   The Monte Capanne pluton thus shows clear similarities with the Aegean plutons. Figure

465   12 shows a simplified scheme of the geometrical and kinematic relations between detachments

466   and plutons based on the examples of the Aegean and the Northern Tyrrhenian, modified from

467   Rabillard et al. (2018). The root zone of the pluton, characterized with an association of mafic

468   and acidic magmas, shows a steeper upward magmatic flow and evidence of co-magmatic

469   stretching and shearing parallel to the regional direction of extension with a kinematics similar

470   to that of the main detachments. During the emplacement of the pluton, the magma chamber

471   progressively opens toward the surface and the granitoids evolve toward finer-grained facies.

472   Progressive extension and exhumation is accompanied by the inflation of the pluton and

473   injection of dykes across the ductile detachment. New detachments are formed above

474   sequentially.

475

476   **5.2.   *A conceptual model based on published numerical experiments***

477

478   This evolution can be compared with numerical models. Thompson and Connolly (1995)

479   summarize the three ways of melting lower continental crust as (1) supplying water to the crust

480   to lower the solidus, (2) decreasing pressure and (3) providing additional heat to the lower crust.

481   They also state that extension alone of a thickened crust is unlikely to reach the conditions of

482   lower crustal melting unless some additional heat is given by the mantle. Back-arc regions

483   above retreating slabs, where the lithosphere is thinned and the asthenosphere advected upward

484   underneath the crust seem to the first order to fit these conditions (Roche et al., 2018).

485   Schubert et al. (2013) have explored numerically the effect of the injection of molten

486   mafic material in an extending crust. They show that the injection of this hot material in the

487   lower crust will induce melting and trigger the formation of felsic magmas that will then ascent

488   along steep normal faults all the way to the upper crust, forming the observed plutons. This is

489   a situation that can easily be compared with the Aegean or the Tuscan archipelago where the

490   granitoids are associated in their root zones with coeval mafic magmas and the felsic plutons

491   ascend along low-angle detachments. In figure 13, we propose a further conceptual model based

492   on numerical experiments of post-orogenic extensional deformation with low-angle shear zones

493   (Huet et al., 2011).
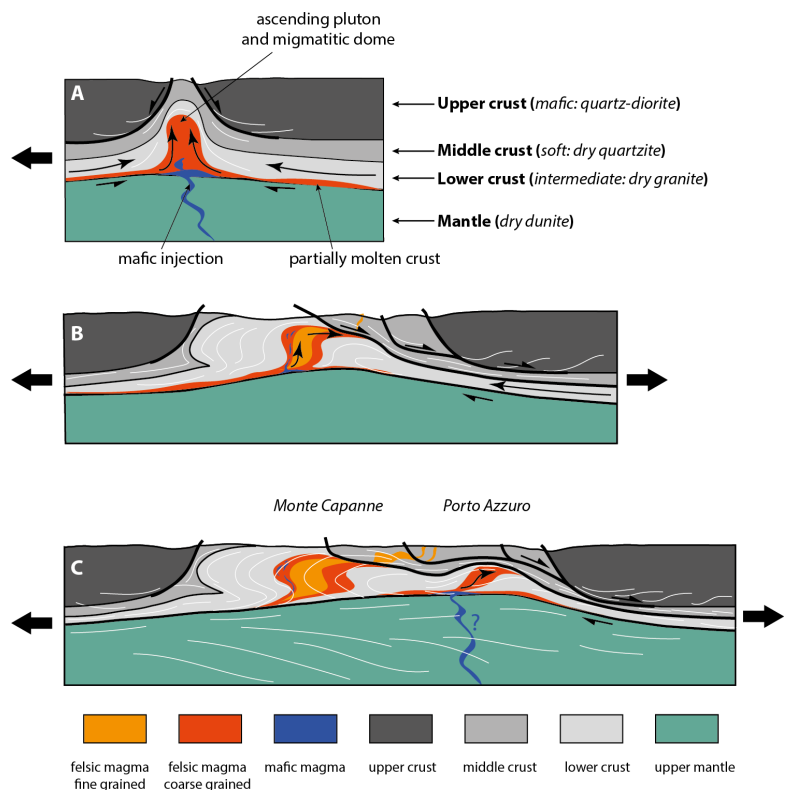
494

495   *Figure 13: Conceptual model of the succession of events leading to the emplacement of a*
496   *plutonic system below an active series of detachments, based on Huet et al. (2011) and*
497   *Schubert et al. (2013).*

498

499

500   In this series of numerical experiments, the thermal gradient and Moho temperature were
501   varied as well the rheological stratification with either a classical rheological stratification or
502   an inverted crustal structure resulting from the formation of the pre-extension nappe stack, the
503   latter setup being used in figure 13, see also Labrousse et al. (2016) for more details on the
504   dynamics of this system with inverted rheological profiles. This latter choice is designed to
505   mimic the Aegean orogenic wedge where the Cycladic Blueschists Unit is sandwiched between
506   the Cycladic Basement and the Upper Cycladic Unit (UCU) (Huet et al., 2009; Jolivet and Brun,
507   2010; Ring et al., 2010). The UCU belongs to the Pelagonian paleogeographic domain and is
508   largely composed of an ophiolite, denser and stronger than the CBU (Labrousse et al., 2016) as
509   well as other basement lithologies (Reinecke et al., 1982; Katzir et al., 1996; Soukis and
510   Papanikolaou, 2004; Martha et al., 2016; Lamont et al., 2020). Asymmetric lateral boundary
511   conditions are applied with 1 cm/yr on the left side and no displacement of the right side as in
512   Tirel et al. (2004). The upper surface is free and the base is driven by hydrostatic forces. No
513   prescribed discontinuity is introduced in the model, strain localization is only due to the use of
514   random noise in the cohesion value of the upper crust (for more details, see Huet et al., 2011).
515   The results shown here represent a case where the rheological stratification is inverted and the
516   thermal gradient is high, a likely situation in the Aegean or Tyrrhenian post-orogenic and back-
517   arc contexts.

518   The conceptual model of the interactions between the numerical model dynamics and the
519   intrusions is that we assume that a batch of mafic magmas, issued from partial melting of the
520   mantle, is injected at the base of the lower crust where it triggers the melting of felsic materials.
521   This leads to the formation of migmatites and collection of the felsic melts in a rising pluton
522   progressively caught in the detachment dynamics as it reaches the upper parts of the crust. The
523   felsic magma is thus deformed while it is still partly liquid and then mylonitized once it has
524   cooled down below the solidus. While extension proceeds, the overburden is removed by the
525   activity of the detachment and the molten material that comes next is injected in lower pressure
526   conditions and finds a faster access to the surface because of extension, thus leading to smaller
527   grainsize plutonic facies and probable volcanism at the surface. While the system of
528   detachments migrates toward the right and a new dome forms, the same situation can be
529   reproduced and a new pluton is emplaced below a detachment further to the right, closer to the
530   active detachment. This evolution is reminiscent of the evolution of Elba Island with the
531   formation of the Monte Capanne pluton in a first stage and the Porto Azzuro pluton in a later
532   stage.

533

534 ### *5.3.   Testing the concept with numerical experiment*

535

536   This conceptual model is now tested with new numerical experiments involving the

537 emplacement of magmas like in Schubert et al. (2013), but in a different situation where low-

538 angle detachments form, to see whether the introduction of a low-viscosity material in the

539 model developed by Huet et al. (2011) would drastically change the system dynamics or not.

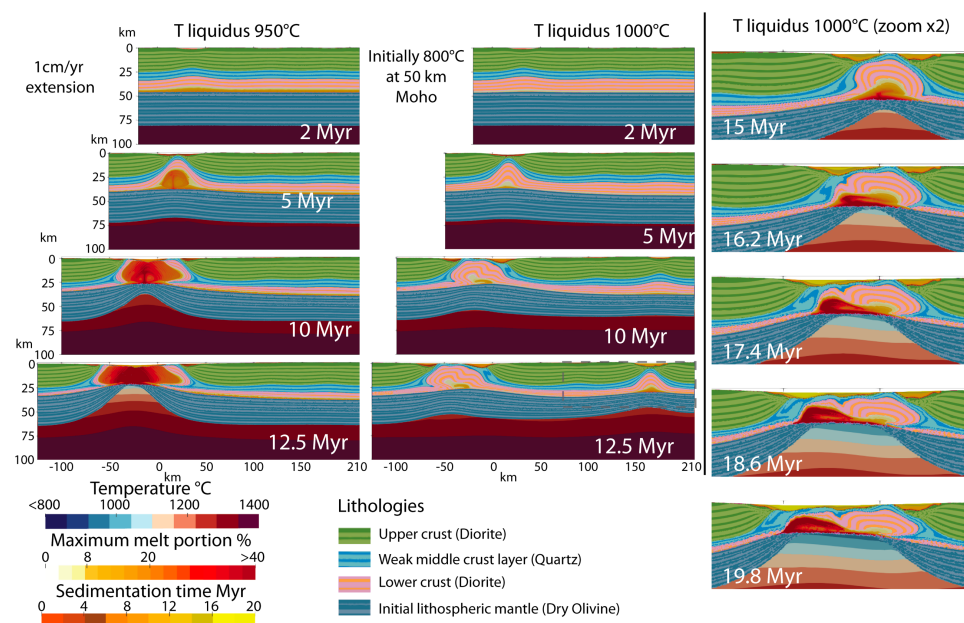540 This has been done for figures 14, 15 and 16.

541

542 *Figure 14: Snapshots of the numerical experiments with two different liquidus temperatures*
543 *(950°C and 1000°C) from 2 to 12.5 Myr. White line limits the molten lower crust with melt*
544 *ration above 40% (pluton).*

545

546   The kinematics of exhumation produced by the nappe stacking experiments of Huet et al.

547 (2011) produces extension along long-lived detachment better resembling Mediterranean

548 example than diapiric spreading models that are produced by models with no intermediate weak

549 layers as in Tirel et al. (2004, 2008) or Rey et al. (2009). Hence, in order to test how molten

550 rocks interacts with detachments, we decided to build on our experience and start from this set

551 up which is a 210 km wide model domain submitted to 1cm/yr of extension on its left side for

552 10 Myr or more with an initial lithospheric column constituted from 25 km upper crust, 10 km

553 weak middle crust, 15 km thick lower crust overlying 40 km of lithospheric mantle. The Moho

554 located at 50 km depth is initially at a temperature of 830°C. We have taken the same

555   rheological parameters which are reported in Table A1 (Appendix A). The four major

556   differences with Huet et al. (2011) are :

557

558   i)   Erosion and sedimentation applied on the top boundary,

559   ii)   the deforming Wrinkler foundation at the LAB has been replaced by inflow of

560   asthenospheric material with higher thermal diffusivity to simulate small scale

561   convection and keep the base of the lithosphere at 1300°C during the experiments

562   as it was the case in Huet et al. (2011) study,

563   iii)   the numerical code used in this study is pTatin2d (May et al., 2014, 2015) that solves

564   the same momentum equation

565    $$\nabla . \sigma = \rho g$$

566   For velocity v, as well as heat conservation

567

568    $$-\nabla . (-\kappa \nabla T + vT) + H = \frac{\partial T}{\partial t}$$

569

570   for Temperature T as Huet et al. (2011). However, it uses an incompressible visco-plastic

571   rheology minimizing the stress between a dislocation creep regime and Drucker Prager failure

572

573    $$\nabla . v = 0$$
       $$\sigma = min \left(\sin \phi + 2\, C \cos \phi \,, \dot{\varepsilon}^{\frac{1}{n}} A^{\frac{-1}{n}} e^{\frac{Q+VP}{nRT}} \right)$$

574

575   to evaluate an effective viscosity :

576    $$\eta_r = \frac{\sigma}{2\dot{\varepsilon}}.$$

577

578   instead of visco-elasto-plastic rheology based on dislocation creep and Mohr Coulomb failure

579   criteria.

580

581   iv)   We added a simplified parametrization in order to account for the mechanical effect

582   of a melt in the simulations. The melt fraction M_f has been introduced as a linear

583   function of solidus (T_s) and liquidus (T_l) temperature

584

585    $$M_f = min \left(max \left(\frac{T - T_s}{T_l - T_s}, 0 \right), 1 \right)$$

586

587 following Gerya and Yuen (2003). Based on melt fraction, the density and viscosity of passive

588 markers are modified following algebraic averaging for density

589

590 $$\rho = M_f \rho_m + (1 - M_f)\rho_r,$$

591

592 and harmonic averaging for viscosity

593

594 $$\eta = \left(\frac{M_f}{\eta_m} + \frac{1 - M_f}{\eta_r}\right)^{-1}.$$

595

596 The solidus dependence on pressure P (in GPa) is implemented following wet granite

597 solidus of Miller et al. (2003), but we also added a variable temperature offset ΔT to account

598 for more mafic granitic composition as follows:

599

600 $$T_s^c = 590 + \frac{250}{10(P + 0.1)} + \Delta T$$

601

602 and the dependence of liquidus to pressure is modeled following:

603

604 $$T_l^c = T_s^c|_{P=0} + 10 + 200P.$$

605

606 The mantle is also allowed to melt following Hirshmann et al. (2000) solidus law

607

608 $$T_s^m = -5.904P^2 + 139.44P + 1108.08$$

609 $$T_l^m = T_s^m + 600$$

610

611 All solidus and liquidus are represented on figure A2 (Appendix A) as a function of

612 pressure and temperature. For low melting temperature of the lower crust (wet granite solidus

613 with ΔT up to 100°C), the crust is largely molten in the initial conditions and buoyancy effects

614 dominate forming "spreading domes" in the classification of Huet et al. (2011), and this despite

615 the presence of a weak middle crustal layer. For higher melting temperature (ΔT from 150°C)

616 melt proportion remains below the 8% melt connectivity threshold described by Rosenberg

617 and Handy (2005) during most of the simulation. We interpret elements with markers that never

618   crossed that critical threshold as migmatites. In that case, melting does not disrupt the typical

619   asymmetric detachment kinematics observed in Elba and in the Cyclades that was well

620   reproduced by Huet et al. (2011) study. In the late stage of deformation, when the lithospheric

621   mantle is sufficiently attenuated by boudinage, the temperature of the lower crust reaches a

622   sufficient temperature to melt more generously, generating plutons which we define as markers

623   with a melt proportion greater than 40%.
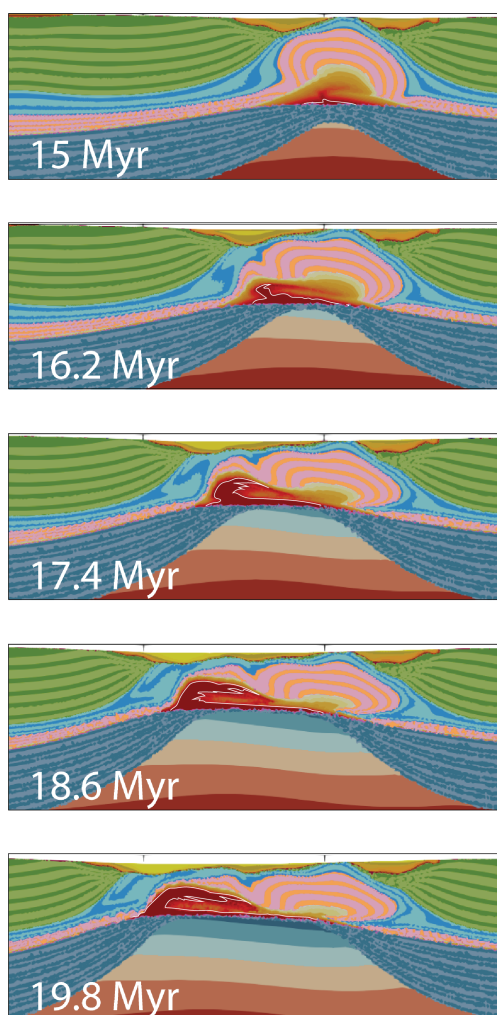
624

625   *Figure 15: Zoom of the last 5 Ma of evolution of the model of figure 15 with a liquidus*
626   *temperature of 1000°C from 15Myr to 19.8 Myr (black dotted rectangle on figure 15 for*
627   *location).*

628

629

630   With a temperature of 950°C at the surface for the liquidus, the molten layer is initially

631   thicker (figure 14) and strain develops into a spreading dome geometry like in the models of

632   Tirel et al. (2004, 2008) or Rey et al. (2009), with symmetric strain pattern and limited strain

633   localization. Shear is indeed progressively relocalized on newly formed shear zones at the top

634   of newly exhumed hot material at the structure axis. When the temperature of the liquidus is

635   higher, reaching 1000°C in surface conditions (figure 14), the molten layer is initially thinner,

636   the deformation is persistently more localized on a detachment on one edge of the dome

637   structure and the model evolves with a detachment on the side of a dome with a limited rate of

638   partial melting in the lower crust (<8%). The deformation ultimately migrates to form a second

639   dome where a syn-kinematic low viscosity body develops with a melt ratio >40%, which we

640   interpret as analogous to a granite intrusion. The late evolution of this second dome shows a

641   strongly asymmetric geometry with the shape of the syn-kinematic intrusion controlled by the

642   asymmetry in strain pattern and a low-angle shear zone (figure 15). Figure 16 shows a structural

643   interpretation of the final step of the model for the second dome highlighting this asymmetry:

644   the dome is bounded by two antithetic crustal scale persistent shear zones, with steep and

645   shallow dip, and an eccentricity of the intrusion feeding pipe within the dome. This overall

646   asymmetrical strain and intrusion localization in the case of limited partial melting rate hence

647   reproduces the main features of the strain and intrusion pattern described in the field in the

648   Cyclades and Elba.
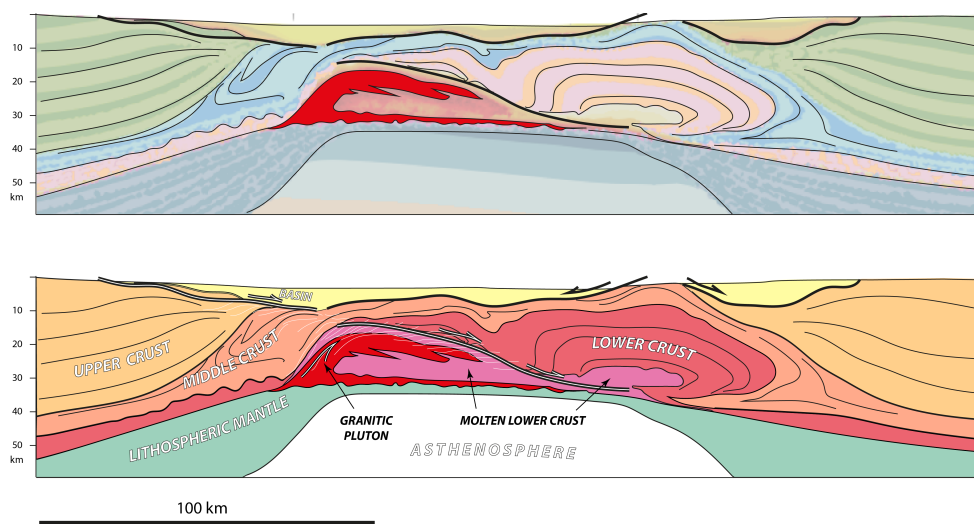
649

650   *Figure 16: Structural cross-section based on the most evolved stage of the numerical model at*
651   *19.8 Myr.*

652

653

654   Although the model does not show the details of the interactions between the dome and

655 the pluton, which involve percolation of melts, drainage through migmatites and dyke-swarms,

656 and progressive intrusion of the detachment by the rising granite, the overall geometry and

657 kinematics is similar with the natural case. The observed geometry is better reproduced in runs

658 with higher crustal melting temperatures and limited melt production. Low temperature melting

659 reactions for the continental crust are the wet solidus and the muscovite dehydration solidus,

660 while biotite and hornblende dehydration melting reactions could represent higher temperature

661 melting reactions (Weinberg and Hasalová, 2015). The model does not show either the role of

662 mafic injections at the base of the model. In the case of the Aegean and Monte Capanne, we

663 have postulated that mafic melts, generated by partial melting of the mantle in the arc and back-

664 arc region, intrude the lower crust and trigger the generation of felsic melts that then rise within

665 the dome. This is an additional input of heat in the model that would also localize the weakest

666 layers and thus the deformation and likely favor the evolution of the model in the same direction

667 as in the model presented here with a lower melting temperature. Similar evolution can arise

668 with an additional input of water in the lower crust. This water may originate from amphibole-

669 rich gabbros (sanukitoides) that could act as water donors enhancing lower crustal partial

670 melting to further produce secondary I-type granites (Castro, 2020). In the Aegean arc, whereas

671 amphibole bearing, I-type granites (Naxos and Serifos granodiorites among others) likely

672 reassemble secondary I-type granites as described by Castro et al. (2020 and references therein),

673 this water origin remains elusive as amphibole-bearing mantle magmas are not yet evidenced

674 interacting with the migmatites, except in the Mykonos-Delos-Rheneia MCC (Jolivet et al.,

675 2021).

676   The metamorphic parageneses associated with contact metamorphism in the case of Elba

677 suggests a depth of emplacement of the pluton of 4-5 km. In the numerical model, the genesis

678 of the pluton starts in the lower crust at a larger depth. The contact metamorphism observed in

679 the field characterizes the upper part of the pluton after it had risen within the crust, which may

680 explain this apparent contradiction.

681   One additional factor has not been considered in this study, the heterogeneity of the crust

682 inherited from earlier tectonic events. It has been shown by numerical experiments that dipping

683 heterogeneities in the crust mimicking structures inherited from nappe stacking help localizing

684 deformation, favoring the development of asymmetrical extensional structures and the

685 development of MCCs (Le Pourhiet et al., 2004; Huet et al., 2011; Lecomte et al., 2011; 2012).

686 Using this sort of initial conditions with melting would also favor the localization of

687 deformation on a single detachment. It may alternatively favor the development of several
688 asymmetric domes with low-angle detachments. Future studies should focus on testing such
689 initial conditions and also test these processes in 3-D.

690 The comparison of the Aegean and North Tyrrhenian plutons shows that the model of
691 interactions between plutons and detachments proposed by Rabillard et al. (2018) is
692 reproducible in similar contexts in different regions and can thus be probably generalized. The
693 comparison of this field-based conceptual model with numerical models moreover suggests that
694 this conceptual model is physically feasible. It requires the concomitance of post-orogenic
695 extension, thus extension set on an orogenic wedge, and a back-arc context to provide the
696 necessary heat and water for the generation of magmas in the mantle and the crust. The
697 possibility of a slab tear would be even more favorable as it increases the possibilities of
698 advecting hot asthenosphere directly below the extending crust (Roche et al., 2018).

699 As shown in the 3-D numerical experiments of Roche et al. (2018), slab retreat and back-
700 arc extension lead to the boudinage of the lithosphere with a spacing of ~100 km which will
701 then localize the formation of crustal domes and detachments. This type of evolution may
702 explain the formation of the lines of domes observed in the Aegean and the Menderes Massif.
703 Whether the boudinage also focuses the collection of mantle-derived magmas below the domes
704 is a question that should be addressed by further modelling. This question is important also
705 because the interactions between plutons and detachments described here and in Rabillard et
706 al. (2018) may provide guides for geothermal exploration. The case of the Menderes Massif is
707 exemplary of the intimate relations between active geothermal fields and crustal-scale
708 detachments (Roche et al., 2018). The case of the Tuscan Archipelago is partly similar with the
709 geothermal fields of Larderello and Monte Amiata developed above recent shallow plutons in
710 a context of asymmetric extension with top-to-the east low-angle shear zones (Jolivet et al.,
711 1998; Brogi et al., 2003; Rochira et al., 2018). The Monte Capanne and Porto Azzuro plutons
712 on Elba are associated with hydrothermal activities and mineralization (Maineri et al., 2003;
713 Rossetti and Tecce, 2008; Liotta et al., 2015) that make them good exhumed analogues of active
714 geothermal fields, a situation that is found also in the Cyclades with the mineralizations
715 observed on Mykonos or Serifos in the Cyclades (Salemink, 1985; St. Seymour et al., 2009;
716 Menant et al., 2013; Tombros et al., 2015; Ducoux et al., 2016).

717

718 **6. Conclusions**

719

720 The comparison between the Aegean and Tyrrhenian Miocene plutons shows striking
721 similarities in their interactions with coeval detachments. These plutons were all emplaced
722 underneath low-angle ductile shear zones and brittle detachments in a post-orogenic back-arc
723 environment where extra heat is provided by advected asthenospheric mantle. The roots of
724 those felsic plutons show a mixing with mafic magmas. The magmatic fabric is steep in the
725 vicinity of the roots and shallows toward the detachments. The plutons record substantial
726 stretching and shearing coaxial with the regional deformation while they still contain a
727 significant amount of melt. In sub-solidus conditions, the granitoids are then mylonitized when
728 approaching the detachment, until the formation of ultra-mylonites and pseudotachylytes. In
729 both cases too, the felsic magma intrudes the detachment and invades the upper plate. A
730 migration of detachments is then observed from the deep and ductile detachments to more
731 brittle and surficial ones. Late magmatic batches show a smaller grain size compatible with an
732 opening of the magma chamber toward the surface suggestive of the volcano-plutonic context
733 of these plutons. To account for these similarities suggesting that this model can be generalized
734 we proposed a conceptual model where mafic magmas batches are injected in the lower crust
735 of an extending orogenic wedge in a back-arc region with low-angle detachments. These mafic
736 injections trigger the melting of the lower crustal felsic material and the ascent of felsic plutons
737 in the crust, controlled by the low-angle detachments. The migration of the detachments through
738 time explains the migration of plutons and detachments observed in the Tuscan Archipelago
739 and in Tuscany from the Late Miocene to the Late Pliocene, as well as in the Aegean. This
740 conceptual model is tested with a numerical approach showing the impact of melt supply in the
741 development of the dome strain pattern. The observed asymmetry of strain localization and
742 intrusion are reproduced for a limited melting rate, while a higher melting rate would lead to
743 the development of a completely different dome structure. The geometry and kinematics
744 observed in the field are well reproduced by the model. These intimate interactions between
745 plutons and detachments can be foreseen as useful guides for the prospection and understanding
746 of geothermal and associated mineralization.

747 **Author contribution**: Laurent Jolivet, Laurent Arbaret, Florent Cheval-Garabedian, Vincent
748 Roche and Aurélien Rabillard did the field work in the Aegean, Loïc Labrousse and Laetitia Le
749 Pourhiet designed the modeling procedure and ran the numerical experiments. All authors
750 contributed to the writing of the manuscript.

751 **Competing interests**: The authors declare that they have no conflict of interest.

755 # References

756

757 Angelier, J., Glaçon, G., Muller, C., 1978. Sur la présence et la position tectonique du Miocène
758   inférieur marin dans l'archipel de Naxos (Cyclades, Grèce). C. R. Acad. Sc. Paris 286,
759   21-24.

760 Avanzinelli, R., Lustrino, M., Mattei, M., Melluso, L., Conticelli, S., 2009. Potassic and
761   ultrapotassic magmatism in the circum-Tyrrhenian region: Significance of carbonated
762   pelitic vs. pelitic sediment recycling at destructive plate margins. Lithos 113, 213–227;
763   doi:210.1016/j.lithos.2009.1003.1029.

764 Barberi, F., Giglia, G., Innocenti, F., Marinelli, G., Raggi, G., Ricci, C.A., Squarci, P., Taffi,
765   L., Trevisan, L., 1967. Carta geologica dell' isola d'Elba scala 1:25000. C.N.R. Roma.

766 Bargnesi, E.A., Stockli, D.F., Mancktelow, N., Soukis, K., 2013. Miocene core complex
767   development and coeval supradetachment basin evolution of Paros, Greece, insights from
768   (U–Th)/He   thermochronometry.   Tectonophysics   595-596,   165-182,
769   dx.doi.org/110.1016/j.tecto.2012.1007.1015.

770 Beaudoin, A., Augier, R., Laurent, V., Jolivet, L., Lahfid, A., Bosse, V., Arbaret, L., Rabillard,
771   A., Menant, A., 2015. The Ikaria high-temperature Metamorphic Core Complex
772   (Cyclades, Greece): Geometry, kinematics and thermal structure. Journal of
773   Geodynamics 92, 18-41, http://dx.doi.org/10.1016/j.jog.2015.1009.1004.

774 Berger, A., Schneider, D.A., Grasemann, B., Stockli, D., 2013. Footwall mineralization during
775   Late Miocene extension along the West Cycladic Detachment System, Lavrion, Greece.
776   Terra Nova 25, 181-191, doi: 110.1111/ter.12016.

777 Berthé, D., Choukroune, P., Jegouzo, P., 1979. Orthogneiss, mylonite and non coaxial
778   deformation of granites : the example of the South Armorican Shear Zone. J. Struct.
779   Geol. 1, 31-42.

780 Bessière, E., Rabillard, A., Précigout, J., Arbaret, L., Jolivet, L., Augier, R., Menant, A.,
781   Mansard, N., 2017. Strain localization within a syn-tectonic intrusion in a back-arc
782   extensional context: the Naxos monzogranite (Greece). Tectonics 37, DOI:
783   10.1002/2017TC004801.

Solid Earth
Discussions

Open Access

784 Bianco, C., Brogi, A., Caggianelli, A., Giorgetti, G., Liotta, D., Meccheri, M., 2015. HP-LT
785   metamorphism in Elba Island: Implications for the geodynamic evolution of the inner
786   Northern Apennines (Italy). Journal of Geodynamics 91, 13-25;
787   http://dx.doi.org/10.1016/j.jog.2015.1008.1001.

788 Bianco, C., Godard, G., Halton, A., Brogi, A., Liotta, D., Caggianelli, A., 2019. The lawsonite-
789   glaucophane blueschists of Elba Island (Italy). Lithos 348-349, 105198;
790   https://doi.org/105110.101016/j.lithos.102019.105198.

791 Bolhar, R., Ring, U., Allen, C.M., 2010. An integrated zircon geochronological and
792   geochemical investigation into the Miocene plutonic evolution of the Cyclades, Aegean
793   Sea, Greece: Part 1: Geochronology. Contrib Mineral Petrol 160, 719–742, DOI
794   710.1007/s00410-00010-00504-00414.

795 Bolhar, R., Ring, U., Kemp, A.I.S., Whitehouse, M.J., Weaver, S.D., Woodhead, J.D., Uysal,
796   I.T., Turnbull, R., 2012. An integrated zircon geochronological and geochemical
797   investigation into the Miocene plutonic evolution of the Cyclades, Aegean Sea, Greece:
798   part 2: geochemistry. Contr. Miner. Petrol. 164, 915-933.

799 Bonin, B., 2004. Do coeval mafic and felsic magmas in post-collisional to within-plate regimes
800   necessarily imply two contrasting, mantle and crustal, sources? A review. Lithos 78 1–
801   24; doi:10.1016/j.lithos.2004.1004.1042.

802 Bouillin, J.P., Bouchez, J.L., Lespinasse, P., Pêcher, A., 1993. Granite emplacement in an
803   extensional setting: an AMS study of the magmatic structures of Monte Capanne (Elba,
804   Italy). Earth and Planetary Science Letters 118, 263-279.

805 Bouillin, J.P., Poupeau, G., Sabil, N., 1994. Etude thermo-chronologique de la dénudation du
806   pluton du Monte Capanne (île d'Elbe, Italie) par les traces de fission. Bulletin de la Société
807   Géologique de France 165, 19-25.

808 Brogi, A., Lazzarotto, A., Liotta, D., Ranalli, G., 2003. Extensional shear zones as imaged by
809   reflection seismic lines: the Larderello geothermal field (central Italy). Tectonophysics
810   363, 127-139.

811 Brown, M., 1994. The generation, segregation, ascent and emplacement of granite magma: the
812   migmatite-to-crustally-derived granite connection in thickened orogens. Earth-Science
813   Reviews 36, 83-130.

814 Brown, M., 2007. Crustal melting and melt extraction, ascent and emplacement in orogens :
815   mechanisms and consequences. J. Geol. Soc London 164, 709-730.

816 Brown, M., Solar, G.S., 1998. Shear-zone systems and melts: feedback relations and self-
817   organization in erogenic belts. J. Struct. Geol 20, 211-227.

818   Brunet, C., Monié, P., Jolivet, L., Cadet, J.P., 2000. Migration of compression and extension in
819   the Tyrrhenian Sea, insights from 40Ar/39Ar ages on micas along a transect from Corsica
820   to Tuscany. Tectonophysics 321, 127-155.
821   Buick, I.S., 1991. The late alpine evolution of an extensional shear zone, Naxos, Greece. J.
822   Geol. Soc. 148, 93-103; doi:110.1144/gsjgs.1148.1141.0093.
823   Buick, I.S., Holland, T.J.B., 1989. The P-T-t path associated with crustal extension, Naxos,
824   Cyclades, Greece, in: Daly, J.S. (Ed.), Evolution of metamorphic belts, pp. 365-369;
825   doi:310.1144/GSL.SP.1989 .1043.1101.1132.
826   Camelli, G.M., Dini, I., D, L., 1993. Upper crustal structure of the Larderello geothermal field
827   as a feature of post-collisional extensional tectonics (southern Tuscany, Italy),, ,.
828   Tectonophysics 224, 413-423.
829   Cao, S., Neubauer, F., Bernroider, M., Genser, J., Liu, J., Friedl, G., 2017. Low-grade
830   retrogression of a high-temperature metamorphic core complex: Naxos, Cyclades,
831   Greece.   Geological   Society   of   America   Bulletin   129,   93–117,
832   doi:110.1130/B31502.31501.
833   Chopra, P.N., Paterson, M.S., 1984. The role of water in the deformation of dunite. J. Geophys.
834   Res 89, 7861-7876.
835   Christofides, G., Perugini, D., Koroneos, A., Soldatos, T., Poli, G., Eleftheriadis, G., DelMoro,
836   A., Neiva, A.M., 2007. Interplay between geochemistry and magma dynamics during
837   magma interaction: an example from the Sithonia Plutonic Complex (NE Greece). Lithos
838   95, 243–266.
839   Collettini, C., Barchi, M.R., 2002. A low-angle normal fault in the Umbria region (Central
840   Italy): a mechanical model for the related microseismicity. Tectonophysics 359, 97-115.
841   Collettini, C., Barchi, M R., 2004. A comparison of structural data and seismic images for low-
842   angle normal faults in the Northern Apennines (Central Italy): constraints on activity, in:
843   Alsop, G.I., Holdsworth, R.E., McCaffrey, K.J.W., M Hands (Eds.), Flow processes in
844   faults and shear zones. Geological Society, London, pp. 95-112.
845   Collettini, C., Holdsworth, R.E., 2004. Fault zone weakening and character of slip along low-
846   angle normal faults: insights from the Zuccale fault, Elba, Italy. J. Geol. Soc. London
847   161, 1039-1051.
848   D'Agostino, N., Chamot-Rooke, N., Funiciello, R., Jolivet, L., Speranza, F., 1998. The role of
849   pre-existing thrust faults and topography on the styles of extension in the Gran Sasso
850   range (Central Italy). Tectonophysics 292, 229-254.

851   Daniel, J.M., Jolivet, L., 1995. Detachment faults and pluton emplacement; Elba Island
852   (Tyrrhenian Sea). Bull. Soc. géol. France 166, 341-354.

853   de Saint Blanquat, M., Horsman, M.E., Habert, G., Morgan, S., Vanderhaeghe, O., Law, R.,
854   Tikoff, B., 2011. Multiscale magmatic cyclicity, duration of pluton construction, and the
855   paradoxical relationship between tectonism and plutonism in continental arcs.
856   Tectonophysics 500, 20–33, doi:10.10 16/j.tecto.2009.2012.2009.

857   Denèle, Y., Lecomte, E., Jolivet, L., Lacombe, O., Labrousse, L., Huet, B., Le Pourhiet, L.,
858   2011. Granite intrusion in a metamorphic core complex: the example of the Mykonos
859   laccolith   (Cyclades,   Greece).   Tectonophysics   501,   52-70,
860   doi:10.1016/j.tecto.2011.1001.1013.

861   Dini, A., Innocenti, F., Rocchi, S., Tonarini, S., Westerman, D.S., 2002. The magmatic
862   evolution of the late Miocene laccolith–pluton–dyke granitic complex of Elba Island,
863   Italy. Geol. Mag. 139, 257–279; DOI: 210.1017/S0016756802006556.

864   Duchêne, S., Aïssa, R., Vanderhaeghe, O., 2006. Pressure-Temperature-time Evolution of
865   Metamorphic Rocks from Naxos (Cyclades, Greece): constraints from Thermobarometry
866   and Rb/Sr dating Geodynamica Acta 19, 299-319.

867   Ducoux, M., Branquet, Y., Jolivet, L., Arbaret, L., Grasemann, B., Rabillard, A., Gumiaux, C.,
868   Drufin, S., 2016. Synkinematic skarns and fluid drainage along detachments: The West
869   Cycladic Detachment System on Serifos Island (Cyclades, Greece) and its related
870   mineralization.   Tectonophysics   695,   1-26;
871   http://dx.doi.org/10.1016/j.tecto.2016.1012.1008.

872   Duggen, S., Hoernle, K., Van den Bogaard, P., Garbe-Schönberg, D., 2005. Post-Collisional
873   Transition from Subduction- to Intraplate-type Magmatism in the Westernmost
874   Mediterranean: Evidence for Continental-Edge Delamination of Subcontinental
875   Lithosphere.

876   Duranti, S., Palmeri, R., Pertusati, P.C., Ricci, C.A., 1992. Geological evolution and
877   metamorphic petrology of the sequences of eastern Elba (Complex II). Acta
878   Vulcanologica Marinelli Volume, 213-229.

879   Faccenna, C., Becker, T.W., 2010. Shaping mobile belts by small-scale convection. Nature 465,
880   602-605, doi:610.1038/nature09064.

881   Faccenna, C., Becker, T.W., Auer, L., Billi, A., Boschi, L., Brun, J.P., Capitanio, F.A.,
882   Funiciello, F., Horvàth, F., Jolivet, L., Piromallo, C., Royden, L., Rossetti, F., Serpelloni,
883   E., 2014. Mantle dynamics in the Mediterranean. Reviews of Geophysics 52, 283-332;
884   doi:210.1002/2013RG000444.

885   Farina, F., Dini, A., Innocenti, F., Rocchi, S., Westerman, D.S., 2010. Rapid incremental
886   assembly of the Monte Capanne pluton (Elba Island, Tuscany) by downward stacking of
887   magma sheets. GSA Bulletin 122, 1463–1479; doi: 1410.1130/B30112.30111.

888   Faure, M., Bonneau, M., 1988. Données nouvelles sur l'extension néogène de l'Egée: la
889   déformation ductile du granite miocène de Mykonos (Cyclades, Grèce). *C. R. Acad. Sci.*
890   *Paris* **307**, 1553-1559.

891   Faure, M., Bonneau, M., Pons, J., 1991. Ductile deformation and syntectonic granite
892   emplacement during the late Miocene extension of the Aegean (Greece). Bull. Soc. géol.
893   France 162, 3-12.

894   Fernandez, A., Barbarin, B., 1991. Relative rheology of coeval mafic and felsic magmas: nature
895   of resulting interaction processes and shape and mineral fabric of mafic microgranular
896   enclaves, in: Didier, J., Barbarin, B. (Eds.), Enclaves and Granite Petrology.Development
897   in Petrology, 13 Elsevier, pp. 263–275.

898   Fernández, C., Castro, A., 2018. Mechanical and structural consequences of magma
899   differentiation at ascent conduits: A possible origin for some mafic microgranular
900   enclaves   in   granites.   Lithos   320–321,   49–61;
901   https://doi.org/10.1016/j.lithos.2018.1009.1004.

902   Fernandez, A., Gasquet, D., 1994. Relative rheological evolution of chemically contrasted
903   coeval magmas: example of the Tichka plutonic complex (Morocco). Contribution to
904   Mineralogy and Petrology 116, 316–326.

905   Fernandez, A., Laporte, D., 1984. Signification of low symmetry in magmatic rocks. Journal of
906   structural Geology 13, 337-347.

907   Ferrara, G., Tonarini, S., 1985. Radiometric geochronology in Tuscany : results and problems.
908   Rend. Soc. Ital. Min. Petrol. 40, 111-124.

909   Gagnevin, D., Daly, J.S., Poli, G., 2004. Petrographic, geochemical and isotopic constraints on
910   magma dynamics and mixing in the Miocene Monte Capanne monzogranite (Elba Island,
911   Italy). Lithos 78, 157–195; doi:110.1016/j.lithos.2004.1004.1043.

912   Gagnevin, D., Daly, J.S., Poli, G., 2008. Insights into granite petrogenesis from quantitative
913   assessment of the field distribution of enclaves, xenoliths and K-feldspar megacrysts in
914   the Monte Capanne pluton, Italy. Mineralogical Magazine 72, 925–940; DOI:
915   910.1180/minmag.2008.1072.1184.1925.

916   Gautier, P., Brun, J.P., 1994a. Crustal-scale geometry and kinematics of late-orogenic extension
917   in the central Aegean (Cyclades and Evvia island). Tectonophysics 238, 399-424;
918   doi:310.1016/0040-1951(1094)90066-90063.

919 Gautier, P., Brun, J.P., 1994b. Ductile crust exhumation and extensional detachments in the
920   central Aegean (Cyclades and Evvia islands). Geodinamica Acta 7, 57-85.

921 Gautier, P., Brun, J.P., Jolivet, L., 1993. Structure and kinematics of upper Cenozoic
922   extensional detachement on Naxos and Paros (Cyclades Islands, Greece). Tectonics 12,
923   1180-1194; doi:1110.1029/1193TC01131.

924 Gerya, T., Yuen, D., 2003. Rayleigh-Taylor instabilities from hydration and melting propel
925   'cold plumes' at subduction zones. Earth Planet. Sci. Lett. 212, 47-62.

926 Grasemann, B., Petrakakis, K., 2007. Evolution of the Serifos Metamorphic Core Complex.
927   Journal of the Virtual Explorer 27, 1-18.

928 Hansen, F.D., Carter, N.L., 1982. Creep of selected crustal rocks at 1000 MPa. Trans. Am.
929   Geophys. Union 63, 437.

930 Hirschmann, M.M., 2000. Mantle solidus: experimental constraints and the effects of peridotite
931   composition. Geochem. Geophys. Geosyst 1, 2000GC000070.

932 Huet, B., Labrousse, L., Jolivet, L., 2009. Thrust or detachment? Exhumation processes in the
933   Aegean: insight from a field study on Ios (Cyclades, Greece). Tectonics 28, TC3007,
934   doi:3010.1029/2008TC002397.

935 Huet, B., Le Pourhiet, L., Labrousse, L., Burov, E., Jolivet, L., 2011. Post-orogenic extension
936   and metamorphic core complexes in a heterogeneous crust: the role of crustal layering
937   inherited from collision. Application to the Cyclades (Aegean domain). Geophysical J.
938   Int. 184, 611–625, doi: 610.1111/j.1365-1246X.2010.04849.x.

939 Huet, B., Le Pourhiet, L., Labrousse, L., Burov, E., Jolivet, L., 2011. Formation of metamorphic
940   core complex in inherited wedges: a thermomechanical modelling study. Earth Planet.
941   Sci. lett. doi:10.1016/j.epsl.2011.07.004.

942 Innocenti, F., Westerman, D.S., Rocchi, S., Tonarini, S., 1997. The Montecristo monzogranite
943   (Northern Tyrrhenian Sea, Italy): a collisional pluton in an extensional setting. Geological
944   Journal 32, 131-151.

945 Jansen, J.B.H., 1977. Metamorphism on Naxos, Greece. Utrecht University.

946 Jolivet, L., Augier, R., Faccenna, C., Negro, F., Rimmele, G., Agard, P., Robin, C., Rossetti,
947   F., Crespo-Blanc, A., 2008. Subduction, convergence and the mode of backarc extension
948   in the Mediterranean region. Bull Soc géol France 179, 525-550.

949 Jolivet, L., Brun, J.P., 2010. Cenozoic geodynamic evolution of the Aegean region. Int. J. Earth
950   Science 99, 109–138, DOI: 110.1007/s00531-00008-00366-00534.

951 Jolivet, L., Faccenna, C., 2000. Mediterranean extension and the Africa-Eurasia collision.
952   Tectonics 19, 1095-1106; doi:1010.1029/2000TC900018.

953   Jolivet, L., Faccenna, C., Goffé, B., Mattei, M., Rossetti, F., Brunet, C., Storti, F., Funiciello,
954   R., Cadet, J.P., Parra, T., 1998. Mid-crustal shear zones in post-orogenic extension: the
955   northern Tyrrhenian Sea case. J. Geophys. Res. 103, 12123-12160; doi:12110.11029/
956   12197JB03616.

957   Jolivet, L., Lecomte, E., Huet, B., Denèle, Y., Lacombe, O., Labrousse, L., Le Pourhiet, L.,
958   Mehl, C., 2010. The North Cycladic Detachment System. Earth and Planet. Sci. Lett. 289
959   87-104, doi:110.1016/j.epsl.2009.1010.1032.

960   Jolivet, L., Menant, A., Sternai, P., Rabillard, A., Arbaret, L., Augier, R., Laurent, V.,
961   Beaudoin, A., Grasemann, B., Huet, B., Labrousse, L., Le Pourhiet, L., 2015. The
962   geological signature of a slab tear below the Aegean. Tectonophysics 659 166–182, 166–
963   182, doi:110.1016/j.tecto.2015.1008.1004.

964   Jolivet, L., Sautter, V., Moretti, I., Vettor, T., Papadopoulou, Z., Augier, R., Denèle, Y.,
965   Arbaret, L., 2021. Anatomy and evolution of a migmatite-cored extensional metamorphic
966   dome and interaction with syn-kinematic intrusions, the Mykonos-Delos-Rheneia MCC.
967   Journal of Geodynamics, accepted.

968   Juteau, M., Michard, A., Zimmermann, J.L., Albarede, F., 1984. Isotopic heterogeneities in the
969   granitic intrusion of Monte Capanne (Elba island, Italy) and dating concepts. Journal of
970   Petrology 25, 532-545.

971   Katzir, Y., Matthews, A., Garfunkel, Z., Schliestedt, M., Avigad, D., 1996. The tectono-
972   metamorphic evolution of a dismembered ophiolite (Tinos, Cyclades, Greece). Geol.
973   Mag. 133, 237-254.

974   Keay, S., Lister, G., Buick, I., 2001. The timing of partial melting, Barrovian metamorphism
975   and granite intrusion in the Naxos metamorphic core complex, Cyclades, Aegean Sea,
976   Greece. Tectonophysics 342, 275-312; doi:210. 1016/S0040-1951(1001)00168-00168.

977   Keller, J.V., Pialli, G., 1990. Tectonics of the island of Elba: a reappraisal. Boll. Soc. Geol. It.
978   109, 413-425.

979   Keller, J.V.A., Minelli, G., Pialli, G., 1994. Anatomy of late orogenic extension: the Northern
980   Apennines case. Tectonophysics 238, 275-294.

981   Kruckenberg, S.C., Vanderhaeghe, O., Ferré, E.C., Teyssier, C., Whitney, D.L., 2011. Flow of
982   partially molten crust and the internal dynamics of a migmatite dome, Naxos, Greece:
983   internal dynamics of the Naxos dome. Tectonics 30, 1–24, doi:10.1029/2010TC002751.

984   Kuhlemann, J., Frisch, W., Dunkl, I., Kázmér, M., Schmiedl, G., 2004. Miocene siliciclastic
985   deposits of Naxos Island: Geodynamic and environmental implications for the evolution
986   of the southern Aegean Sea (Greece), in: Bernet, M., Spiegel, C. (Eds.), Detrital

987   thermochronology - Provenance analysis, exhumation, and landscape evolution of
988   mountain belts:. Geological Society of America, pp. 51-65.
989   Labrousse, L., Huet, B., Le Pourhiet, L., Jolivet, L., Burov, E., 2016. Rheological implications
990   of extensional detachments: Mediterranean and numerical insights. Earth-Science
991   Reviews 161, 233-258; http://dx.doi.org/210.1016/j.earscirev.2016.1009.1003.
992   Lamont, T.N., Roberts, N.M.W., Searle, M.P., Gopon, P., Waters, D.J., Millar, I., 2020. The
993   age, origin, and emplacement of the Tsiknias Ophiolite, Tinos, Greece. Tectonics 39,
994   e2019TC00567; https://doi.org/ 00510.01029/02019TC005677.
995   Laurent, V., Beaudoin, A., Jolivet, L., Arbaret, L., Augier, R., Rabillard, A., 2015. Interrelations
996   between extensional shear zones and synkinematic intrusions: The example of Ikaria
997   Island (NE Cyclades, Greece). Tectonophysics 651-652, 152-171,
998   http://dx.doi.org/110.1016/j.tecto.2015.1003.1020.
999   Lee, J., Lister, G.S., 1992. Late Miocene ductile extension and detachment faulting, Mykonos,
1000   Greece. Geology 20, 121-124; doi:110.1130/0091-7613(1992)1020<0121:L
1001   MDEAD>1132.1133.CO;1132.
1002   Le Pourhiet, L., Burov, E., Moretti, I., 2004. Rifting through a stack of inhomogeneous thrusts
1003   (the dipping pie concept). Tectonics 23, doi:10.1029/2003TC001584.
1004   Lecomte, E., Le Pourhiet, L., Lacombe, O., 2012. Mechanical basis for the activity of low angle
1005   normal faults. Geophysical Res. Lett. 39, L03307; doi:03310.01029/02011GL050756.
1006   Lecomte, E., Le Pourhiet, L., Lacombe, O., Jolivet, L., 2011. A continuum mechanics approach
1007   to quantify brittle strain on weak faults: application to the extensional reactivation of
1008   shallow-dipping discontinuities. Geophys. J. Int. 184, 1-11, doi: 10.1111/j.1365-
1009   1246X.2010.04821.x.
1010   Liotta, D., Brogi, A., Meccheri, M., Dini, A., Bianco, C., Ruggieri, G., 2015. Coexistence of
1011   low-angle normal and high-angle strike- to oblique-slip faults during Late Miocene
1012   mineralization in eastern Elba Island (Italy). Tectonophysics 660, , 17-34;
1013   http://dx.doi.org/10.1016/j.tecto.2015.1006.1025.
1014   Lister, G.S., Baldwin, S., 1993. Plutonism and the origin of metamorphic core complexes.
1015   Geology 21, 607-610; doi:610.1130/0091-7613(1993)1021<0607:PA
1016   TOOM>1132.1133.CO;1132.
1017   Lister, G.S., Snoke, A.W., 1984. S-C mylonites. Journal of Structural Geology 6, 617-638.
1018   Maineri, C., Benvenuti, M., Costagliola, P., Dini, A., Lattanzi, P., Ruggieri, G., Villa, I.M.,
1019   2003. Sericitic alteration at the La Crocetta deposit (Elba Island, Italy): interplay between

Solid Earth
Discussions
Open Access

1020   magmatism, tectonics and hydrothermal activity. Mineralium Deposita 38, 67–86; DOI
1021   10.1007/s00126-00002-00279-00122.

1022 Martha, S.O., Dörr, W., Gerdes, A., Petschick, R., Schastok, J., Xypolias, P., Zulauf, G., 2016.
1023   New structural and U–Pb zircon data from Anafi crystalline basement (Cyclades,
1024   Greece): constraints on the evolution of a Late Cretaceous magmatic arc in the Internal
1025   Hellenides. International Journal of Earth Sciences 105, 2031–2060,
1026   doi:2010.1007/s00531-00016-01346-00538.

1027 Menant, A., Jolivet, L., Augier, R., Skarpelis, N., 2013. The North Cycladic Detachment
1028   System and associated mineralization, Mykonos, Greece: insights on the evolution of the
1029   Aegean domain. Tectonics 32, 433–452, doi:410.1002/tect.20037.

1030 Miller, C.F., McDowell, S.M., Mapes, R.W., 2003. Hot and cold granites? Implications of
1031   zircon saturation temperatures and preservation of inheritance. Geology 31, 529-532.

1032 Musumeci, G., Vaselli, L., 2012. Neogene deformation and granite emplacement in the
1033   metamorphic units of northern Apennines (Italy): Insights from mylonitic marbles in the
1034   Porto Azzurro pluton contact aureole (Elba Island). Geosphere 8, 470–490;
1035   doi:410.1130/GES00665.00661.

1036 Pandeli, E., Giusti, R., Elter, F.M., Orlando, A., Orti, L., 2018. Structural setting and
1037   metamorphic evolution of a contact aureole: the example of the Mt. Capanne pluton (Elba
1038   Island, Tuscany, italy). Ofioliti 43, 41-73; doi: 10.4454/ofioliti.v4443i4451.4455.

1039 Paterson, S.R., 2009. Magmatic tubes, pipes, troughs, diapirs, and plumes: Late-stage
1040   convective instabilities resulting in compositional diversity and permeable networks in
1041   crystal-rich magmas of the Tuolumne batholith, Sierra Nevada, California. Geosphere 5,
1042   496–527; doi: 410.1130/GES00214.00211.

1043 Pauselli, C., Ranalli, G., 2017. Effects of lateral variations of crustal rheology on the occurrence
1044   of post- orogenic normal faults: The Alto Tiberina Fault (Northern Apennines, Central
1045   Italy). Tectonophysics 721, 45-55; http://dx.doi.org/10.1016/j.tecto.2017.1009.1008.

1046 Pe-Piper, G., 2000. Origin of S-type granites coeval with I-type granites in the Hellenic
1047   subduction system, Miocene of Naxos, Greece. European Journal of Mineralogy 12, 859–
1048   875, doi:810.1127/ejm/1112/1124/0859.

1049 Pe-Piper, G., Kotopouli, C.N., Piper, D.J.W., 1997. Granitoid rocks of Naxos, Greece: regional
1050   geology and petrology. Geological Journal 32, 153–171, doi:110.1002/(SICI)1099-
1051   1034(199706)199732: 199702<199153::AID-GJ199737>199703.199700.CO;199702-
1052   199701.

1053   Pe-Piper, G., Piper, D.J.W., 2002. The igneous rocks of Greece. The anatomy of an orogen.
1054   Gebrüder Borntraeger, Berlin-Stuttgart.

1055   Pe-Piper, G., Piper, D.J.W., 2007. Neogene back-arc volcanism of the Aegean: new insights
1056   into the relationship between magmatism and tectonics, in: Beccaluva, L., Bianchini, G.
1057   (Eds.), Cenozoic Volcanism in the Mediterranean Area. Geological Society of America,
1058   pp. 17–31, doi: 10.1130/2007.2418(1102).

1059   Pe-Piper, G., Piper, D.J.W., Matarangas, D., 2002. Regional implications of geochemistry and
1060   style of emplacement of Miocene I-type diorite and granite, Delos, Cyclades, Greece.
1061   Lithos 60, 47–66, doi:10.1016/S0024-4937(1001)00068-00068.

1062   Perrin, M., 1975. L'ile d'Elbe et la limite Alpes-Apennins: données sur la structure géologique
1063   et l'évolution tectogénétique de l'Elbe alpine et de l'Elbe apennine. Bull. Soc. Geol. It. 94,
1064   1929-1955.

1065   Pertusati, P.C., Raggi, G., Ricci, C.A., Duranti, S., Palmeri, R., 1993. Evoluzione post-
1066   collisionale dell'Elba centro-orientale. Mem. Soc. Geol. It. 49, 297-312.

1067   Perugini, D., Poli, G., Rocchi, S., 2005. Development of viscous fingering between mafic and
1068   felsic magmas: evidence from the Terra Nova Intrusive Complex (Antarctica).
1069   Mineralogy and Petrology 83, 151–166.

1070   Petrakakis, K., Iglseder, C., Zámolyi, A., Rambousek, C., Grasemann, B., Draganitis, E., Kurka,
1071   A., Photiades, A., 2010. Serifos Island, Geological Map of Greece. Institute of Geology
1072   and Mineral Exploration (IGME).

1073   Poli, G., Manetti, P., Tommasini, S., 1989. A petrological review on Miocene–Pliocene
1074   intrusive rocks from Southern Tuscany and Tyrrhenian Sea (Italy). Periodico di
1075   Mineralogia 58, 109 – 126.

1076   Poli, G.E., Tommasini, S., 1991. Model for the Origin and Significance of Microgranular
1077   Enclaves in Calc-alkaline Granitoids. Journal of Petrology 32, 657-666.

1078   Rabillard, A., Arbaret, L., Jolivet, L., Le Breton, N., Gumiaux, C., Augier, R., Grasemann, B.,
1079   2015. Interactions between plutonism and detachments during Metamorphic Core
1080   Complex formation, Serifos Island (Cyclades, Greece). Tectonics 34, 1080-1106, DOI:
1081   1010.1002/2014TC003650.

1082   Rabillard, A., Jolivet, L., Arbaret, L., Bessière, E., Laurent, V., Menant, A., Augier, R.,
1083   Beaudoin, A., 2018. Synextensional Granitoids and Detachment Systems Within
1084   Cycladic Metamorphic Core Complexes (Aegean Sea, Greece): Toward a Regional
1085   Tectonomagmatic Model. Tectonics 37; https://doi.org/10.1029/2017TC004697.

1086 Ranalli, G., Murphy, D.C., 1987. Rheological stratification of the lithosphere. Tectonophysics
1087   132, 281-295.

1088 Reinecke, T., Altherr, R., Hartung, B., Hatzipanagiotou, K., Kreuzer, H., Harre, W., Klein, H.,
1089   Keller, J., Geenen, E., Böger, H., 1982. Remnants of a late Cretaceous high temperature
1090   bet on the island of Anafi (Cyclades, Greece). N. Jb. Miner. Abh 145, 157-182.

1091 Rey, P.F., Teyssier, C., Whitney, D.L., 2009. The Role of Partial Melting and Extensional
1092   Strain Rates in the Development of Metamorphic Core Complexes. Tectonophysics 477,
1093   135-144, doi: 110.1016/j.tecto.2009.1003.1010.

1094 Ring, U., 2007. The geology of Ikaria Island: The Messaria extensional shear zone, granites
1095   and the exotic Ikaria nappe. Journal of the Virtual Explorer 27, 1–32.

1096 Ring, U., Glodny, J., Will, T., Thomson, S., 2010. The Hellenic Subduction System: High-
1097   Pressure Metamorphism, Exhumation, Normal Faulting, and Large-Scale Extension.
1098   Annu. Rev. Earth Planet. Sci. 38, 45–76, 10.1146/annurev.earth.050708.170910.

1099 Rocchi, S., Westerman, D.S., Dini, A., Innocenti, F., Tonarini, S., 2002. Two-stage growth of
1100   laccoliths at Elba Island, Italy. Geology 30, 983–986.

1101 Roche, V., Sternai, P., Guillou-Frottier, L., Menant, A., Jolivet, L., Bouchot, V., Gerya, T.,
1102   2018. Emplacement of metamorphic core complexes and associated geothermal systems
1103   controlled by slab dynamics. Earth and Planetary Science Letters 498 322–333;
1104   https://doi.org/310.1016/j.epsl.2018.1006.1043.

1105 Rochira, F., Caggianelli, A., de Lorenzo, S., 2018. Regional thermo-rheological field related to
1106   granite emplacement in the upper crust: implications for the Larderello area (Tuscany,
1107   Italy). Geodinamica Acta 30, 225-240, DOI: 210.1080/09853111.09852018.01488912.

1108 Rodríguez, C., Castro, A., 2019. Origins of mafic microgranular enclaves and enclave swarms
1109   in granites: Field and geochemical relations. GSA Bulletin 131, 635–660;
1110   https://doi.org/610.1130/B32028.32021.

1111 Rosenberg, C.L., Handy, M.R., 2005. Experimental deformation of partially melted granite
1112   revisited: implications for the continental crust. Journal of metamorphic Geology 23

1113 Rossetti, F., Balsamo, F., Villa, I.M., Bouybaouenne, M., Faccenna, C., Funiciello, R., 2008.
1114   Pliocene-Pleistocene HT-LP metamorphism during multiple granitic intrusions in the
1115   southern branch of the Larderello geothermal field (southern Tuscany, Italy). J. Geol.
1116   Soc. London 165, 247-262.

1117 Rossetti, F., Faccenna, C., Jolivet, L., Funiciello, R., Goffé, B., Tecce, F., Brunet, C., Monié,
1118   P., Vidal, O., 1999. Structural signature and exhumation P-T-t path of the Gorgona
1119   blueschist sequence (Tuscan Archipelago, Italy). Ofioliti 26, 175-186.

1120   Rossetti, F., Faccenna, C., Jolivet, L., Tecce, F., Funiciello, R., Brunet, C., 1999b. Syn- versus
1121   post-orogenic extension in the Tyrrhenian Sea, the case study of Giglio Island (Northern
1122   Tyrrhenian Sea, Italy). Tectonophysics 304, 71-93; doi:10.1016/S0040-
1123   1951(1098)00304-00307.

1124   Rossetti, F., Tecce, F., 2008. Composition and evolution of fluids during skarn development in
1125   the Monte Capanne thermal aureole, Elba Island, central Italy. Geofluids 8 167–180; doi:
1126   110.1111/j.1468-8123.2008.00215.x.

1127   Rossetti, F., Tecce, F., Billi, A., Brilli, M., 2007. Patterns of fluid flow in the contact aureole
1128   of the Late Miocene Monte Capanne pluton (Elba Island, Italy): the role of structures and
1129   rheology. Contrib Mineral Petrol 53, 743–760; DOI 710.1007/s00410-00006-00175-
1130   00413.

1131   Salemink, J., 1985. Skarn and ore formation at Serifos, Greece, as a consequence of
1132   granodiorite intrusion. University of Utrecht, Netherlands.

1133   Sanchez-Gomez, M., Avigad, D., Heiman, A., 2002. Geochronology of clasts in allochthonous
1134   Miocene sedimentary sequences on Mykonos and Paros islands: implications for back-
1135   arc extension in the Aegean Sea. J. Geol. Soc. London 159, 45-60; doi:10.1144/0016-
1136   764901031.

1137   Saupé, F., Marignac, C., Moine, B., Sonet, J., Zimmermann, J.L., 1982. Datation par les
1138   méthodes K/Ar et Rb/Sr de quelques roches de la partie orientale de l'ile d'Elbe (Province
1139   de Livourne, Italie). Bulletin de Minéralogie 105, 236-245.

1140   Savelli, C., 1988. Late Oligocene to Recent episodes of magmatism in and around the
1141   Tyrrhenian Sea: implication for the process of opening in a young inter-arc basin of intra-
1142   orogenic (Mediterranean) type. Tectonophysics 146, 163-181.

1143   Savelli, C., 2002a. Tectono-magmatic lineaments and subduction in the central Mediterranean
1144   and southern Italy during the past 8 Ma. Boll. Soc. Geol. It., 121, 231-242.

1145   Savelli, C., 2002b. Time–space distribution of magmatic activity in the western Mediterranean
1146   and peripheral orogens during the past 30 Ma (a stimulus to geodynamic considerations).
1147   Journal of Geodynamics 34, 99–126.

1148   Savelli, C., 2015. Fast Episodes of West- Mediterranean-Tyrrhenian Oceanic Opening and
1149   Revisited Relations with Tectonic Setting. Scientific Reports 5:, 14271; DOi:
1150   14210.11038/srep14271.

1151   Scheffer, C., Vanderhaeghe, O., Lanari, P., Tarantola, A., Ponthus, L., Photiades, A., France,
1152   L., 2016. Syn- to post-orogenic exhumation of metamorphic nappes: Structure and

1153   thermobarometry of the western Attic-Cycladic metamorphic complex (Lavrion, Greece).

1154   Journal of Geodynamics 96, 174–193; http://dx.doi.org/110.1016/j.jog.2015.1008.1005.

1155   Schubert, M., Driesner, T., Gerya, T.V., Ulmer, P., 2013. Mafic injection as a trigger for felsic

1156   magmatism: A numerical study. Geochem. Geophys. Geosyst. 14, 1910–1928,

1157   doi:1910.1002/ggge.20124.

1158   Serri, G., Innocenti, F., Manetti, P., 1993. Geochemical and petrological evidence of the

1159   subduction of delaminated Adriatic continental lithosphere in the genesis of the Neogene-

1160   Quaternary magmatism of central Italy. Tectonophysics 223, 117-147.

1161   Seward, D., Vanderhaeghe, O., Siebenaller, L., Thomson, S., Hibsch, C., Zingg, A., Holzner,

1162   P., Ring, U., Duchêne, S., 2009. Cenozoic tectonic evolution of Naxos Island through a

1163   multi-faceted approach of fission-track analysis, in: Ring, U., Wernicke, B. (Eds.),

1164   Extending a continent: architecture, rheology and heat budget. Geological Society,

1165   London, pp. 179-196; doi:110.1144/SP1321.1149.

1166   Soukis, K.I., Papanikolaou, D.J., 2004. Contrasting geometry between Alpine and Late-to-post-

1167   Alpine tectonic structures in Anafi Island (Cyclades). Bulletin of the Geological Society

1168   of Greece vol. 2004 XXXVI, 1688-1696.

1169   Spakman, W., Wortel, R., 2004. A tomographic view on Western Mediterranean geodynamics,

1170   in: Cavazza, W., Roure, F.M., Spakman, W., Stampfli, G.M., Ziegler, P.A. (Eds.), The

1171   TRANSMED Atlas - The Mediterranean region from crust to Mantle. Springer, Berlin,

1172   Heidelberg, pp. 31-52.

1173   St. Seymour, K., Zouzias, D., Tombros, S., Kolaiti, E., 2009. Geochemistry of the Serifos

1174   pluton (Cycladic islands) and associated iron oxide and sulfide ores: Skarn or

1175   metamorphosed exhalite deposits? Neues Jahrbuch für Mineralogie - Abhandlungen 186,

1176   249-270; doi:210.1127/0077-7757/2009/0143.

1177   Thompson, A.B., Connolly, J.A.D., 1995. Melting of the continental crust: some thermal and

1178   petrological constraints on anatexis in continental collision zones and other tectonic

1179   settings. J. Geoph. Res. 100, 15565-15579.

1180   Tirel, C., Brun, J.P., Burov, E., 2004. Thermo-mechanical modeling of extensional gneiss

1181   domes, in: Whitney, D.L., Teyssier, C., Siddoway, C.S. (Eds.), Gneiss domes in orogeny,

1182   Boulder, Colorado, pp. 67-78.

1183   Tirel, C., Brun, J.P., Burov, E., 2008. Dynamics and structural development of metamorphic

1184   core complexes. J. Geoph. Res. 113, doi:10.1029/2005JB003694.

1185   Tombros, S.F., St. Seymour, K., Williams-Jones, A.E., Zhai, D., Liu, J., 2015. Origin of a

1186   barite-sulfide ore deposit in the Mykonos intrusion, cyclades: Trace element, isotopic,

1187   fluid inclusion and raman spectroscopy evidence. Ore Geology Reviews 67, 139–157;
1188   http://dx.doi.org/110.1016/j.oregeorev.2014.1011.1016.

1189 Trevisan, L., 1950. L'Elba orientale e la sua tettonica scivolamento par gravità. Mem. Instit.
1190   Geol. It. Pavia 70, 435-470.

1191 Urai, J.L., Shuiling, R.D., Jansen, J.B.H., 1990. Alpine deformation on Naxos (Greece), in:
1192   Knipe, R.J., Rutter, E.H. (Eds.), Deformation mechanisms, Rheology and tectonics. *Geol.*
1193   *Soc. spec. Pub.*, pp. 509-522; doi:510.1144/GSL.SP.1990.1054.1101.1147.

1194 van der Laan, S.R., Wyllie, P.J., 1993. Experimental Interaction of Granitic and Basaltic
1195   Magmas and Implications for Mafic Enclaves. Journal of Petrology 34, 491-517.

1196 Vanderhaeghe, O., 2004. Structural development of the Naxos migmatite dome, in: Whitney,
1197   D.L., Teyssier, C., Siddoway, C.S. (Eds.), Gneiss domes in orogeny. Geological Society
1198   of America, Boulder, Colorado, pp. 211-227.

1199 Vanderhaeghe, O., 2009. Migmatites, granites and orogeny: Flow modes of partially-molten
1200   rocks and magmas associated with melt/solid segregation in orogenic belts.
1201   Tectonophysics 477, 119–134, doi:110. 1016/j.tecto.2009.1006.1021.

1202 Vanderhaeghe, O., Kruckenberg, S.C., Gerbault, M., Martin, L., Duchêne, S., Deloule, S., 2018.
1203   Crustal-scale convection and diapiric upwelling of a partially molten T orogenic root
1204   (Naxos dome, Greece). Tectonophysics 746; https://doi.org/10.1016/j.tecto.2018.03.007,
1205   459–469

1206 Vernon, R.H., 1986. K-feldspar megacrysts in granites - phenocrysts, not porphyroblasts. Earth-
1207   Sci. Rev. 23, 1-63.

1208 Vernon, R.H., Paterson, S.R., 2008. How late are K-feldspar megacrysts in granites? Lithos
1209   104, 327–336; doi:310.1016/j.lithos.2008.1001.1001.

1210 Weinberg, R.F., Hasalová, P., 2015. Water-fluxed melting of the continental crust: A review.
1211   Lithos 212–215, 158–188; http://dx.doi.org/110.1016/j.lithos.2014.1008.1021.

1212 Weinberg, R.F., Sial, A.N., Pessoa, R.R., 2001. Magma flow within the Tavares pluton,
1213   Northeastern Brazil: compositional and thermal convection. Bull. Geol. Soc. Am. 113,
1214   508–520.

1215 Westerman, D.S., Dini, A., Innocenti, F., Rocchi, S., 2004. Rise and fall of a nested Christmas-
1216   tree laccolith complex, Elba Island, Italy, in: Breitkreuz, C., Petford, N. (Eds.), Physical
1217   geology of high level magmatic systems. Geological Society, London, pp. 195-213.

1218 Westerman, D.S., Innocenti, F., Tonarini, S., Ferrara, G., 1993. The Pliocene intrusions of the
1219   island of Giglio. Mem. Soc. Geol. It. 49, 345-363.

1220   Wiebe, R.A., Jellinek, A.M., Hodge, K.F., 2017. New insights into the origin of ladder dikes:
1221   Implications for punctuated growth and crystal accumulation in the Cathedral Peak
1222   granodiorite. Lithos 277, 241–258; http://dx.doi.org/210.1016/j.lithos.2016.1009.1015.
1223   Wortel, M.J.R., Spakman, W., 2000. Subduction and slab detachment in the Mediterranean-
1224   Carpathian region. Science 290, 1910-1917.
1225
1226

Appendix A Table A1

1227

1228

		Sediments (2)	Upper crust (1)	Middle crust(2)	Lower crust(1)	Lithospheric mantle(3)	Asthenospheric mantle(3)
Density(kg.m^{-3})	ρ_r	2400	2700	2700	2700	3300	3300
Pre exp. Factor (MPa^{-n}s^{-1})	A	2.4	3.3	2.4	3.3	3.5	3.5
Activation energy(kJ)	Q	156	186	156	219	532	532
Stress exponent	n	6.7 10^{-6}	2 10^{-6}	6.7 10^{-6}	1.3 10^{-3}	2.5 10^{4}	2.5 10^{4}
Melt density(kg.m^{-3})	ρ_m	-	2400	2400	2400	2800	2800
Melt viscosity	η_m	-	10^{17}	10^{17}	10^{17}	10^{12}	10^{12}
Heat production (Wm^{-3})	H	1.67 10^{-10}	1.67 10^{-10}	0	0	0	0
Thermal diffusivity	κ	10^{-6}	10^{-6}	10^{-6}	10^{-6}	10^{-6}	5 10^{-6}

1229

1230 *Table A1 : Values and notation for variable physical parameters. Parameters for dislocation*

1231 *creep come from 1 (Ranalli and Murphy, 1987), 2 (Hansen and Carter, 1982) and 3 (Chopra*

1232 *and Paterson, 1984). Other constant parameters include: friction ϕ and cohesion C which*

1233 *varies linearly with plastic strain in range [0,1] respectively from 30° to 20° and from 20*

1234 *MPas to 2 MPa; Coefficient of thermal expansion and compressibility that are set to $3.10^{-5}K^{-1}$*

1235 *and 10^{-11} Pa^{-1}.*

1236

Appendix A, figure A1 and A2:
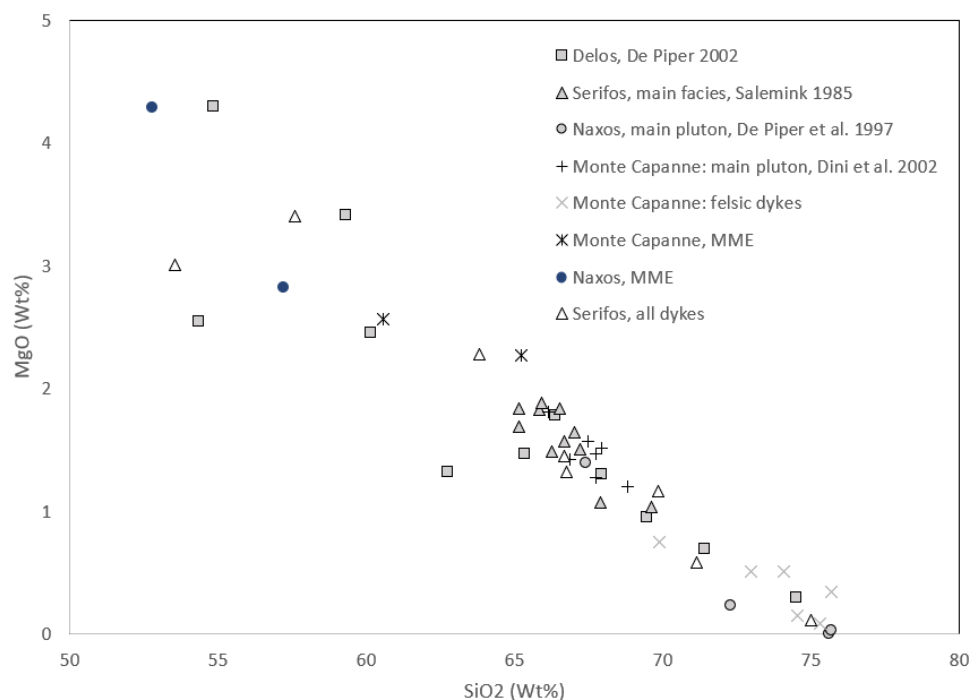
1237

1238

1239

1240

Figure A1: MgO v. Si02 Harker diagram showing the negative correlation between whole rock MgO and SiO2 content for three, I-type hornblende-biotite bearing, representative Aegean granites. Data from Delos intrusion (Pe-Piper et al., 2002), Serifos (Salemink, 1985) and Naxos (Pe-Piper et al., 1997). Mixing/mingling processes between mafic mantle-derived melts and acid magmas produce composite batholiths (Poli and Tommasini, 1990) as illustrated by the case of the Elba Island magmatic complex showed for comparison (See Dini et al. 2002 for explanation). MME = Mafic Microgranular Enclaves.
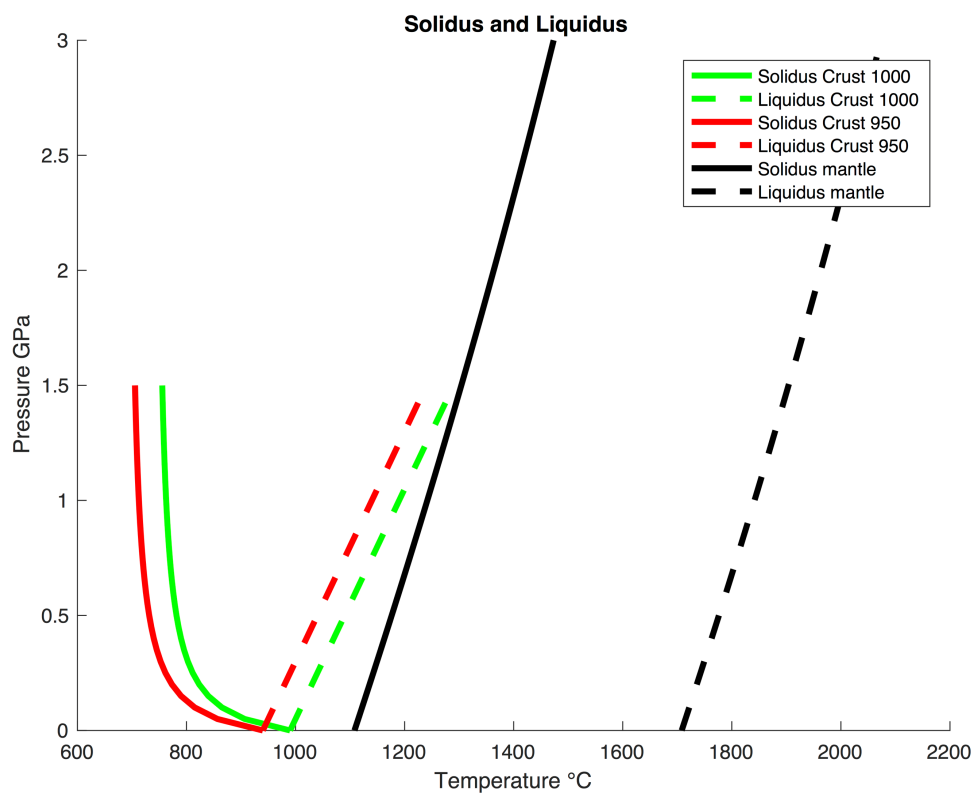
1241
1242
1243
1244
1245
1246
1247
1248

1249

Figure A2: Solidus and liquidus as a function of pressure and temperature for mantle and crust (950 and 1000°C).